



HAL
open science

Contourite on the Limpopo Corridor, Mozambique margin: Long-term evolution, facies distribution and Plio-Quaternary processes

Nathalie Babonneau, François Raison, Adrien Genêt, Ugo Lopes, Ruth Fierens, Elda Miramontes, Sidonie Révillon, Marina Rabineau, Laurence Droz, Deborah Belleney, et al.

► To cite this version:

Nathalie Babonneau, François Raison, Adrien Genêt, Ugo Lopes, Ruth Fierens, et al.. Contourite on the Limpopo Corridor, Mozambique margin: Long-term evolution, facies distribution and Plio-Quaternary processes. *Sedimentology*, 2022, 10.1111/sed.13045 . hal-03871748

HAL Id: hal-03871748










<https://hal.univ-brest.fr/hal-03871748v1>

Submitted on 25 Nov 2022

HAL is a multi-disciplinary open access archive for the deposit and dissemination of scientific research documents, whether they are published or not. The documents may come from teaching and research institutions in France or abroad, or from public or private research centers.

L'archive ouverte pluridisciplinaire **HAL**, est destinée au dépôt et à la diffusion de documents scientifiques de niveau recherche, publiés ou non, émanant des établissements d'enseignement et de recherche français ou étrangers, des laboratoires publics ou privés.

Contourite on the Limpopo Corridor, Mozambique margin: Long-term evolution, facies distribution and Plio-Quaternary processes

NATHALIE BABONNEAU* , FRANÇOIS RAISSON† , ADRIEN GENÊT*,
UGO LOPES*, RUTH FIERENS* , ELDA MIRAMONTES‡ § ,
SIDONIE RÉVILLON* ¶ , MARINA RABINEAU* , LAURENCE DROZ* ,
DEBORAH BELLENEY***, MARYLINE MOULIN*  and DANIEL ASLANIAN* 

*UMR 6538 GEO-OCEAN, Univ Brest, CNRS, Ifremer, Univ. Bretagne-Sud, 29280 Plouzané, France
(E-mail: nathalie.babonneau@univ-brest.fr)

†TotalEnergies, CSTJF, Avenue Larribau, 64000, Pau, France

‡MARUM-Center for Marine Environmental Sciences, University of Bremen, Bremen, 28359, Germany

§Faculty of Geosciences, University of Bremen, Bremen 28359, Germany

¶SEDISOR, place N. Copernic, 29280 Plouzané, France

***UMR 6554, LETG Littoral, Environnement, Télédétection, Géomatique UMR 6554, Institut
Universitaire Européen Mer, UBO, Place Copernic, 29280 Plouzané, France

Associate Editor – Zhifei Liu

ABSTRACT

Bottom currents are key processes that contribute to the shaping of submarine slopes, with the redistribution of sediments in contourite systems. Despite numerous recent studies on contourite systems, the complexity and diversity of these sedimentary systems are still not fully understood and often underestimated. Their understanding requires comprehensive works integrating all scales from seismic architecture to microfacies. This paper focuses on a contouritic ridge located between 2000 m and 2500 m water depth on the Mozambique margin. Bathymetry, seismic data and piston cores collected during the PAMELA-MOZ3 cruise allow a multi-scale study from large depositional geometries to sedimentary facies. At the seismic scale, the contouritic ridge shows three stages of evolution with: (i) initiation and development of the drift/moat system; (ii) an intermediate stage with successive incisions and aggradations; and (iii) moat infill and drift erosion during the Plio-Quaternary. Plio-Quaternary deposits are composed of hemipelagic, turbiditic and contouritic facies filling the moat. Coarse-grained contouritic facies, dominated by planktonic foraminifera, are identified on the western flank of the ridge between the moat infill and the erosional area at the top of the ridge. They consist of condensed deposits, with sedimentation rate about 0.3 cm/ka, indicating a strong and stable bottom current that winnows away the fine-grained component. This facies could be present more generally in an intermediate position between erosion and depositional areas in contourite systems. At present, the contourite system is located at the transition depth between North Atlantic Deep Water and Antarctic Intermediate Water. Trajectories of bottom currents are complex and interact with sporadic turbidity currents and anti-clockwise eddies that participate in reshaping the sea floor morphology. Although Plio-Quaternary depositional geometries indicate the end of drift/moat development, the moat filling and drift erosion are also related to bottom currents and constitute atypical contouritic sedimentation.

Keywords Bottom current, calcarenite, contourite, drift, moat, Mozambique.

INTRODUCTION

For several decades, the sedimentary processes that shape the ocean floor were actively studied. Contourite deposits were the subject of many recent studies, which revealed a significant diversity and complexity (Stow *et al.*, 2002, 2009; Faugères & Stow, 2008; Hernández-Molina *et al.*, 2008a,b; Rebesco *et al.*, 2014, and references therein) that depends on the level of interaction of bottom currents with gravity processes affecting continental margins (Stow & Faugères, 2008; Sansom, 2018; Rodrigues *et al.*, 2022). Concerning sedimentary architecture and morphology of contourite sedimentary systems without direct contribution of gravity processes, studies based on geophysical data and sparse cores indicate that many large contourite drifts on the present sea floor are dominated by muddy or silty sediments (Hernández-Molina *et al.*, 2008a, 2016; Rebesco *et al.*, 2014, and references therein).

First studies on sedimentary facies identified the bi-gradational contourite sequence (Gonthier *et al.*, 1984; Stow *et al.*, 2002) as the standard contourite depositional structure. However, a growing number of studies on sedimentary cores show a great diversity of contouritic facies with muddy or sandy facies, carbonate facies and all intermediate facies between turbidites, hemipelagites and contourites (Stow & Smillie, 2020). Recent works concerning microfacies, ichnofacies, chemical composition and grain size of contourite deposits allow further characterization of sedimentary facies (Bankole *et al.*, 2020; Hüneke *et al.*, 2020; Yu *et al.*, 2020; de Castro *et al.*, 2020a, 2021; Rodrigues *et al.*, 2022). Concentration and accumulation of sand by bottom currents is recognized in different parts of contourite systems, such as in contourite channels, moats, contourite terraces and within muddy contourite drifts (Stow *et al.*, 2002; Miramontes *et al.*, 2016; Brackenridge *et al.*, 2018; Yu *et al.*, 2020). It requires strong bottom currents capable of reworking sandy elements and winnowing finer sediments (de Castro *et al.*, 2021).

Recent work on contourites clearly shows that to make progress in understanding sedimentary objects and processes, it is necessary to examine contourite systems from small-scale sedimentary facies (grain size, laminations, bioturbations) to larger scale features, such as seismic architecture

on continental margins within an oceanographic and climatic context and its evolution (Stow & Smillie, 2020). The scientific approach proposed in this paper integrates all of these scales, illustrating an atypical behaviour of contouritic sedimentation that follows the development of the drift/moat system and leads to its degradation.

The study area is located in the Mozambique Channel where contouritic features were observed and studied at different scales, locations, stratigraphic positions and water depths. Several recent studies address the submarine morphologies in relation to the bottom currents observed in the Mozambique Channel at all water depths, from the shelf break to the deep basin, with or without links to turbidite systems, and around seamounts associated with carbonate platforms (Counts *et al.*, 2018; Fierens *et al.*, 2019; Thiéblemont *et al.*, 2019, 2020; Miramontes *et al.*, 2019a, 2021; de Castro *et al.*, 2021). The cruises supported by the PAMELA project (PASSive Margin Exploration Laboratories) in the Mozambique Channel, and especially the PAMELA-MOZ3 cruise (Moulin & Aslanian, 2016; Moulin *et al.*, 2020), acquired geophysical data and CALYPSO cores on a sedimentary ridge located in the Limpopo Corridor. These data allow a first detailed description of the morphology and recent architecture of the ridge and a characterization of the sedimentary facies in a robust stratigraphic framework.

The aim of this paper is to characterize the variability of sedimentary facies in the Plio-Quaternary deposition of a large contouritic ridge and to interpret the distribution of coarse-grained sedimentary facies. It also presents the evolution of a large drift from its construction to its present degradation by integrating the distribution of sedimentary facies. Finally, it proposes an interpretation of the evolution of bottom currents and a model integrating sedimentary architecture and sedimentary facies coupled with oceanographic processes.

REGIONAL SETTINGS

Geological settings: margin structure and regional sedimentation

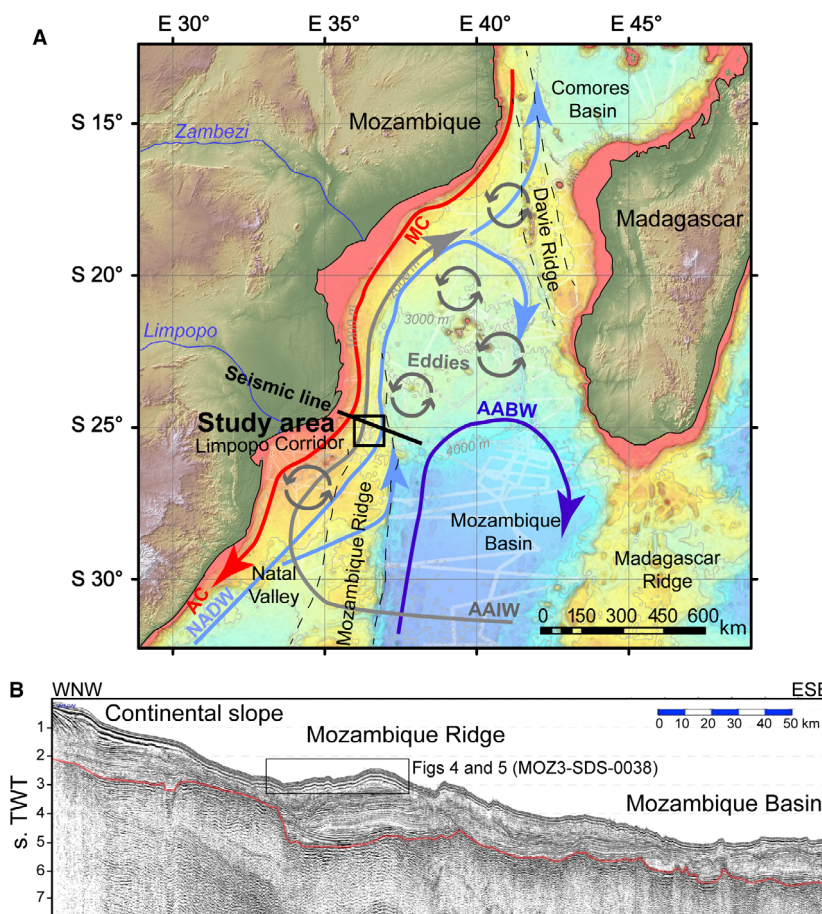
The Mozambique Channel is located in the south-western Indian Ocean, separating Africa

and the island of Madagascar (Fig. 1). With a width of 420 km in the north and 1000 km in the south, the Mozambique Channel includes the southern part of the Somalian Basin in the north and Mozambique Basin in the south, separated by the Davie Ridge. This ridge is a 40 km wide morphological high, extending for about 2000 km between the coasts of Mozambique and Madagascar. It corresponds to the accommodation of the southward displacement of Madagascar from the beginning of the break-up of Gondwana until the Lower Cretaceous (Coffin & Rabinowitz, 1987; Nairn *et al.*, 1991; Mahanjane, 2014; Thompson *et al.*, 2019). Initially subject to a dexterous movement, the Mozambique Channel finally opened by oceanic expansion from the Middle Jurassic, as the Antarctic and Australian continents moved south and eastward away from Africa. South of the Mozambique Coastal Plain, the Natal Valley is a sedimentary basin above a 30 km thick continental crust, 1000 m below sea-level, probably resulting from a subsidence induced by probable

intrusions of mantle-derived melts in the lower crust (Moulin *et al.*, 2020; Evain *et al.*, 2021; Leprêtre *et al.*, 2021).

The Limpopo Corridor lies along the Mozambique Coastal Plain and Natal Valley and shows a north–south aligned series of positive gravity anomalies, in continuity with the one produced by the magmatic Mozambique Ridge, south of the Naude ridge. The Limpopo Corridor was supposed to be floored by oceanic crust, with emplacement during the opening of the Mozambique Basin as a northern extension of the magmatic Mozambique Ridge, south of the Naude ridge (Leinweber & Jokat, 2012; Mueller & Jokat, 2019). Combined wide-angle and multi-channel seismic studies and geodynamic studies have shown that the Limpopo Corridor is a strike-slip margin with thin continental crust (Thompson *et al.*, 2019; Moulin *et al.*, 2020; Evain *et al.*, 2021; Li *et al.*, 2021; Watremez *et al.*, 2021). The positive gravity anomalies correspond to a series of bathymetric highs between 2000 m and 3000 m of water depth (Evain

Fig. 1. (A) Bathymetric map of the Mozambique Channel, showing the main physiographic domains, the study area at the north of the Mozambique Ridge (Limpopo Corridor) and the general oceanographic circulation. From shallow to deep current: Mozambique Current and Agulhas Current (MC and AC; 0 to 900 m), Antarctic Intermediate Water (AAIW; 900 to 1500 m), North Atlantic Deep Water (NADW; 2200 to 3500 m), Antarctic Bottom Water (AABW; 4000 to 4700 m). (B) Regional seismic profile MZ-05 (PAMELA-MOZ3 cruise) across the Limpopo Corridor, where the red line indicates the base of Cretaceous sedimentary basins.



et al., 2021), which were recognized as contourite drifts in seismic surveys (Wiles *et al.*, 2014; Thiéblemont *et al.*, 2019; Gao *et al.*, 2020; Li *et al.*, 2021) overlying mass transport deposits (MTD; Evain *et al.*, 2021). These MTDs may be related to the emplacement of the first bathymetric step, during the passive margin formation. The regional sedimentary succession deposited on the Limpopo Corridor extends from the Barremian to the Holocene. The Barremian to the Aptian is characterized by a series of pre-rift sediments composed of shallow fossil-rich clays. The Aptian then marks the post-rift unconformity (Raillard, 1991). Open marine sedimentation began in the Early Cretaceous for the northern and southern Mozambique basins (Davison & Steel, 2018).

Oceanographic settings

The hydrological and oceanographic context of the Mozambique Channel is complex (Fig. 1A). The geographic location and tropical climate imply a shallow thermocline and marked water column stratification. Several sets of oceanic currents interact; surface currents (0 to 600 m), intermediate currents (600 to 2000 m) and deep currents (2000 to 5000 m; Uenzelmann-Neben & Huhn, 2009).

Surface currents originate from the local tropical climatic and atmospheric regime. The strong winds generated in this part of the world are linked to monsoon phenomena that cause surface water masses to move mainly southward, as the Agulhas Current (AC) and the Mozambique Current (MC), which are western boundary currents forming the greater Agulhas Current system (Lutjeharms, 2006). They both flow along the coast of Africa from north to south (AC and MC in Fig. 1A) at speeds of up to 2 to 3 m/s (Donguy & Piton, 1991; Raillard, 1991).

Intermediate ocean currents are composed of two main water masses; the Red Sea Intermediate Water (RSW) coming from the north, and the Antarctic Intermediate Water (AAIW, 900 to 1500 m interval) coming from the south. De Ruijter *et al.* (2002) describe the southward progression of the RSW within anticyclonic eddies and a mixing between the RSW and the AAIW at the heart of this particular circulation (AAIW in Fig. 1A).

The deep ocean currents are composed of components from global currents such as the North Atlantic Deep Water (NADW, 2200 to 3500 m interval) and the Antarctic Bottom Water (AABW

below 4000 m; NADW and AABW in Fig. 1A). They enter the Mozambique Channel from the south and flow northward along the eastern African margin. A part of the NADW flows into the southern Mozambique Basin across the Limpopo Corridor (Wiles *et al.*, 2014). The AAIW and the upper part of the NADW probably continue to flow northward along the northern Mozambique margin. The lower part of the NADW and the AABW are constrained by the northward decrease in the bathymetry and flow back southward along the western margin of Madagascar (Fig. 1A; van Aken *et al.*, 2004; Ullgren *et al.*, 2012; Charles *et al.*, 2020).

In addition, the region is also affected by large (diameters of ≥ 300 km) cyclonic and anticyclonic eddies (Fig. 1A; Ridderinkhof *et al.* 2010; Halo *et al.*, 2014). The gyres described by these eddies have a diameter of greater than 300 km, can affect the entire water column and reach the sea floor (de Ruijter *et al.*, 2002; Halo *et al.*, 2014; Penven *et al.*, 2014). Their average frequency is four per year for an average migration speed estimated at 4.5 km per day (Schouten *et al.*, 2002, 2003).

Contouritic sedimentary processes in the Mozambique margin

The intense circulation of water masses in the Mozambique Channel widely affects sedimentation and sea floor morphology at all depths, from the shelf (Flemming & Kudrass, 2017) to the deep part of the basin (Kolla *et al.*, 1980; Wiles *et al.*, 2014, 2017; Breitzke *et al.*, 2017; Fierens *et al.*, 2019; Ponte *et al.*, 2019; Miramontes *et al.*, 2019b,c, 2020, 2021). Contourite sedimentary structures (depositional or erosional) were identified in almost the entire Mozambique Channel, from the upper slope and top of seamounts, to the deeper parts of the Mozambique Basin. However, they are more widely developed along the Mozambique margin.

Analysis of two-dimensional multichannel seismic reflection profiles and bathymetric features revealed major contourite systems with erosive, depositional and mixed features, and provided a morpho-sedimentary map, interpreted with hydrographic data and hydrodynamic modelling (Thiéblemont *et al.*, 2019). That study highlighted how the position (depth) of water-mass interfaces constrains the morphology of contourite terraces at regional scale, and how the Limpopo Corridor controls the local water mass behaviours and dynamics (Thiéblemont *et al.*, 2019). Interpretation of seismic

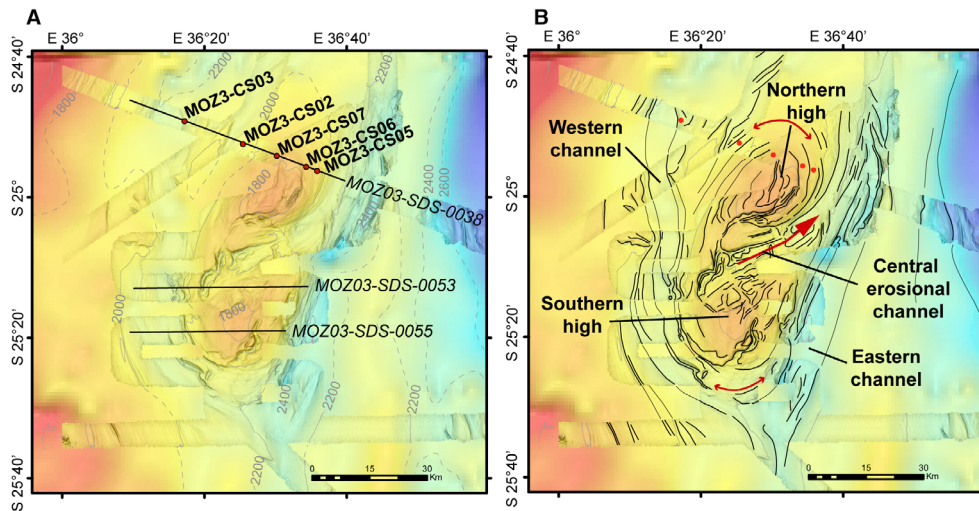


Fig. 2. (A) Detailed bathymetric map (isobaths every 200 m) showing the morphology of the bathymetric highs of the study area. Location of the sediment cores and the CHIRP profiles. (B) Line drawing of the morphological features underlying the two main channels and the erosional structures and possible interpretation of bottom current direction (red arrows).

profiles on the northern part of the Mozambique margin also showed the different evolution stages of the contourite systems from their initiation, with the drift growth stage between 95 to 94 Ma and 25 to 23 Ma, a stability or maintenance stage between 25 to 23 Ma and 17 to 15 Ma and finally, the moat filling stage from 17 to 15 Ma to the present day (Thiéblemont *et al.*, 2020). The end of drift growth and the beginning of moat infilling is correlated with the deepening of Antarctic water bodies caused by the input of the NADW (Thiéblemont *et al.*, 2020).

DATA AND METHODS

The data used in this work were acquired during the PAMELA-MOZ3 and PAMELA-MOZ5 oceanographic cruises in April 2016 on-board the *R/V Pourquoi Pas?* (Moulin & Aslanian, 2016). The database (Fig. 2) consists of a bathymetric dataset, CHIRP sub-bottom profiles and five Calypso cores (piston cores), complemented by the regional seismic profile MZ-05 crossing the Limpopo Corridor (Fig. 1B). This profile was acquired with an array of airguns providing a total volume of 6500-inch³ with a shot interval every 60 s (signal emitted between 10 Hz and 70 Hz), and a 4500 m long multi-channel streamer (720 channels) during the PAMELA-MOZ3 cruise. This seismic profile was

acquired to image the deep structure of the margin and does not resolve the superficial sedimentary layers.

Moreover, a regional multichannel seismic profile was provided by TotalEnergies courtesy of Instituto Nacional de Petroleo (INP) and WesternGeco Multiclient, as partners in the PAMELA project (Fig. 3). This profile provides 3 s TWT (two-way travel time) of thickness of interpretable seismic signal showing the sedimentary structure of the Mozambique ridge at a large scale. The regional seismic survey and the correlations of regional reflectors at a well located 3 km away were taken from the works of Ponte *et al.* (2019) and Thiéblemont *et al.* (2020).

Geophysical data: bathymetry and CHIRP sub-bottom profiler data

The *R/V Pourquoi Pas?* is equipped with a multibeam echosounder (SMF) ©RESON – Seabat 7150 bi-frequency 12/24 kHz (Reson, Slangerup, Denmark). The bathymetric data were processed by IFREMER to obtain a 20 × 20 m resolution grid. They were integrated into a Geographic Information System with all the data from the PAMELA project. For the other areas, the regional GEBCO 2021 bathymetry is used.

CHIRP sub-bottom profiler data were acquired along the multibeam bathymetry surveys of PAMELA-MOZ3 and PAMELA-MOZ5 cruises

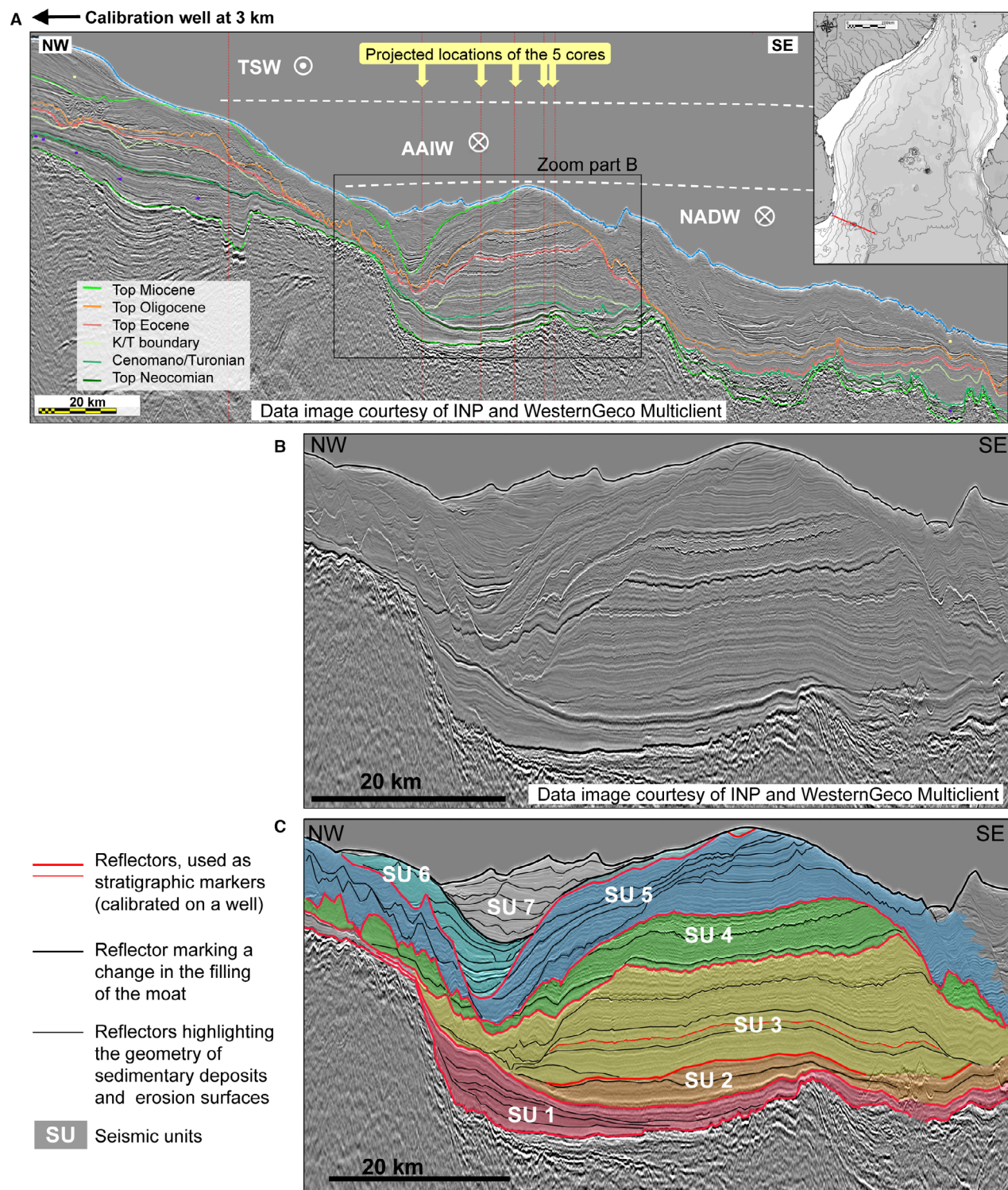


Fig. 3. (A) Regional multichannel seismic profile crossing the Mozambique Ridge (the section represents 6 s TWT). The cores are projected with less than 2.6 km offset. TSW – Tropical Surface Water, AAIW – Antarctic Intermediate Water, NADW – North Atlantic Deep Water; (B) Zoom of the same seismic profile focused on the Mozambique ridge (this zoom represents 3 s TWT); (C) Line-drawing of the zoom with the interpretation of the seven seismic units (coloured areas named SU).

Table 1. List and characteristics of the CALYPSO cores collected during the PAMELA-MOZ3 cruise on the sedimentary ridge.

Core	Latitude	Longitude	Water depth (m)	Core length (m)	Section number
MOZ3-CS02	24°52.441S	36°25.424E	2041	10.66	11
MOZ3-CS03	24°49.195S	36°17.210E	2125	20.06	21
MOZ3-CS04	24°44.287S	35°47.392E	1032	9.44	10
MOZ3-CS05	24°56.280S	36°35.854E	1926	6.35	7
MOZ3-CS06	24°35.685S	36°34.311E	1868	7.89	8
MOZ3-CS07	24°54.129S	36°30.192E	1853	11.47	12

with a signal frequency that varies between 5300 Hz and 1800 Hz. The penetration of the signal in the sediment is variable up to approximately 80 m and the vertical resolution is about 0.75 m.

Core data set, sedimentology and petrography

Five CALYPSO piston cores were collected on the bathymetric high described as a contourite drift (Table 1), during the oceanographic cruise PAMELA-MOZ3. The five cores are located on the seismic CHIRP profile MOZ30032_B (Figs 2 and 4). Sedimentary descriptions were carried out on all the cores, with a particular emphasis on sediment colour, visual grain size and sedimentary structures (laminations, bioturbations), as represented on the sedimentological logs. The visual analysis of sedimentary facies was supplemented by the acquisition of physical parameters and the chemical composition of the sediment, as well as X-ray imaging.

Physical parameters (gamma-density, magnetic susceptibility and P-wave velocity) were acquired with a Multi-Sensor Core-Logger (MSCL; Geotek Limited, Daventry, UK) at Ifremer (Brest, France), with a sampling interval of 1 cm. Spectrocolorimetry was acquired with ©Minolta CM-2600d (Minolta, Osaka, Japan), coupled to the MSCL logger, and the analysis step here is also 1 cm. It provides the colour and luminescence of the sediment, right after the core opening. X-ray radiography (CTscan, Geotek Limited) was also acquired on the core half-sections at Ifremer (Brest, France). It allows the identification of many sedimentary structures invisible to direct observation.

Sediment cores were sampled for grain-size analyses using the Malvern laser grain-size analyser (Mastersizer 2000; Malvern Panalytical, Malvern, UK) at IUEM laboratory (Brest, France), for the 0.01 to 2000 µm fraction. The complete

grain-size distribution of each sample is interpreted. Sample intervals were adapted and chosen according to sedimentary facies. They were not regularly and systematically sampled for laser particle size measurements but targeted on certain sedimentary sections or sequences to characterize depositional types. The sampling step size ranges from 10 to 1 cm in the layers with the most variability (sampling points will be indicated by small white dots on the core photographs in the figures). No chemical pre-treatment was carried out before the measurements (no dissolution of carbonates, no deflocculation and no elimination of organic matter). The particle size curve shows the full range of particles, including a large number of foraminifera, but negligible organic matter content.

The chemical compositions of major elements were obtained with the Avaatech X-ray fluorescence (XRF) core-scanner (Avaatech, BV, Alkmaar, The Netherlands) available at Ifremer. The selected measurement area was 8 mm and the step-size was set at 1 cm. Each core was analysed at 10 kV and 30 kV. More than 25 major elements were measured [elements with an atomic mass between aluminium (Al) and uranium (U)], such as iron (Fe), calcium (Ca), strontium (Sr), rubidium (Rb), titanium (Ti), silicon (Si), sulphur (S) or chlorine (Cl). The results are expressed in counts per second (cps), corresponding to a semi-quantitative measurement of the elements content that can be used to assess the vertical variability of the chemical composition in the core. For the interpretation of these curves in marine sediments, the Ca curve is considered a good indicator of carbonate production. Iron, Al or Rb indicate the terrigenous fraction. The Ca/Fe ratio is often a good indicator between the biogenic marine pole (for example, hemipelagic) and the detrital pole (for example, turbidite) in deep marine deposits (Richter *et al.*, 2006).

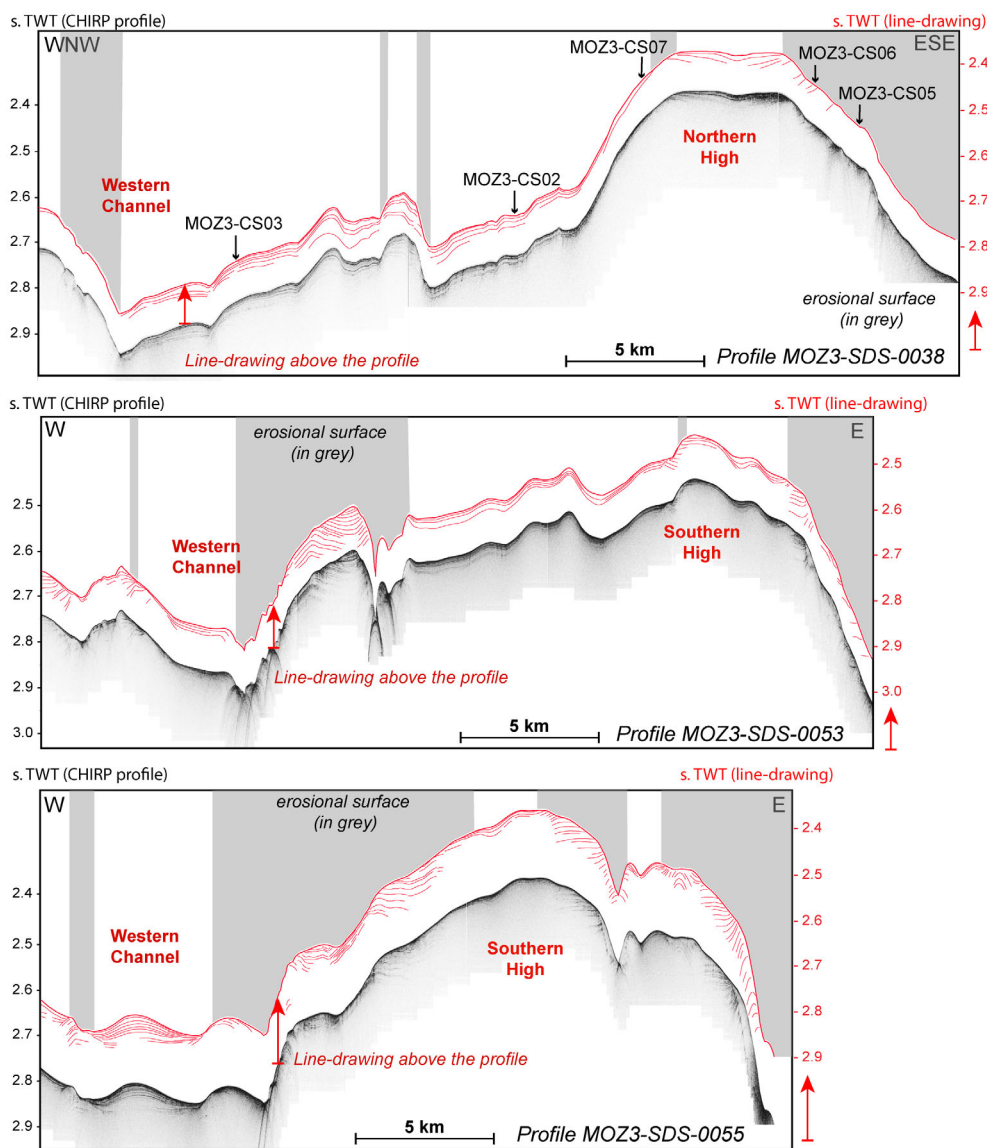


Fig. 4. CHIRP profiles from north to south: MOZ3-SDS-0038, MOZ3-SDS-0053 and MOZ3-SDS-0055 across the ridge (see location in Fig. 3). The layer geometry is underlined by the red line-drawing (above the profile, see the red arrows). Location of the cores on profile MOZ3-SDS-0038.

Microfacies analysis and quantitative mineralogy were performed at TotalEnergies Scientific and Technical Centre (Pau, France) on 26 thin sections (Table 2) with Qemscan[®] technology, which allows inventory, mapping and particle count on the sections. Bulk quantitative mineralogy (BQM) analysis, including elementary composition by X-ray diffraction (DX), density, insoluble residue, loss on ignition and cation exchange capacity measurements were carried out in addition on seven of these samples for calibration. Qemscan[®] and BQM analysis

diverge slightly in a few cases (heavy minerals, quartz content).

Stratigraphy and age models

The age models of sediment cores were obtained by combining several methods: radiocarbon dating, O-isotope analysis on planktonic foraminifera, Sr-isotope analysis on total sediment and correlation of cores *via* XRF data or by using CHIRP profiles. Three AMS radiocarbon datings were obtained on the core MOZ3-CS03 (Table 3).

Table 2. List of samples analysed by Qemscan® (QS) and by quantitative mineralogy (MQ, grey lines).

Sample no.	Core	Depth (mbsf)	Analysis	Sample doubling	Facies
s1	MOZ3-CS03	10.09	QS	–	Foram-rich mudstone
s2	MOZ3-CS03	11.44	QS	–	Bioclastic sand
s3	MOZ3-CS03	12.54	QS		Sand
s4	MOZ3-CS03	13.09	QS	(1)	Bioclastic sand
s5	MOZ3-CS03	13.09	MQ	(2)	Bioclastic sand
s6	MOZ3-CS03	16.05	QS	–	Sand
s7	MOZ3-CS03	16.37	QS	(1)	Bioclastic sand
s8	MOZ3-CS03	16.37	MQ	(2)	Bioclastic sand
s9	MOZ3-CS03	19.45	QS	–	Sand
s10	MOZ3-CS03	19.65	QS	–	Sand
s11	MOZ3-CS02	2.97	QS	–	Bioclastic sand
s12	MOZ3-CS02	3.90	QS	–	Foram-rich mudstone
s13	MOZ3-CS02	6.84	QS	–	Bioclastic sand
s14	MOZ3-CS02	7.68	QS	–	Bioclastic sand
s15	MOZ3-CS02	8.25	QS	–	Bioclastic sand
s16	MOZ3-CS02	9.03	QS	(1)	Bioclastic sand
s17	MOZ3-CS02	9.03	MQ	(2)	Bioclastic sand
s18	MOZ3-CS07	0.33	QS	–	Bioclastic sand
s19	MOZ3-CS07	1.33	QS	(1)	Bioclastic sand
s20	MOZ3-CS07	1.33	MQ	(2)	Bioclastic sand
s21	MOZ3-CS07	2.36	QS	–	Bioclastic sand
s22	MOZ3-CS07	3.33	QS	–	Bioclastic sand
s23	MOZ3-CS07	4.33	QS	–	Bioclastic sand
s24	MOZ3-CS07	5.33	QS	–	Bioclastic sand
s25	MOZ3-CS07	6.30	MQ	(1)	Bioclastic sand
s26	MOZ3-CS07	6.33	QS	(2)	Bioclastic sand
s27	MOZ3-CS07	7.33	QS	–	Bioclastic sand
s28	MOZ3-CS07	8.33	QS	–	Bioclastic sand
s29	MOZ3-CS07	9.33	QS	–	Bioclastic sand
s30	MOZ3-CS07	10.33	QS	(1)	Bioclastic sand
s31	MOZ3-CS07	10.33	MQ	(2)	Bioclastic sand
s32	MOZ3-CS07	11.30	MQ	(1)	Bioclastic sand
s33	MOZ3-CS07	11.33	QS	(2)	Bioclastic sand

For each sample, about 10 mg of *Globigerinoides ruber* was picked out from the >150 mm fraction, washed in an ultrasonic bath with distilled water, and dried. These samples were then

analysed at the Beta Analytics Laboratory (London, UK). Reported radiocarbon ages were corrected for a marine reservoir effect of 400 years and converted to calendar years using CALIB Rev

Table 3. Radiocarbon ages obtained on foraminifera picked in hemipelagic layers (*Globigerinoides ruber*), measured by Beta Analytics Laboratory (London).

Core	Sample (cm)	Analytic number	Species	¹⁴ C data (years)	Error	¹⁴ C Age, 2σ interval (years cal BP)	Average age ¹⁴ C (years)
MOZ3-CS03	35–36	461612	<i>G. ruber</i>	6560	30	6693–7074	6880
MOZ3-CS03	75–76	461613	<i>G. ruber</i>	32 910	210	36 109–37 100	36 586
MOZ3-CS03	110–111	461614	<i>G. ruber</i>	N/D	N/D	N/D	N/D

8.2 (Stuiver *et al.*, 1998) with the calibration curve Marine20 (Heaton *et al.*, 2020), with a regional $\Delta R = -35 \pm 29$ (Maboya *et al.*, 2017). Calibrated kilo years before the present will be referred as ka cal BP.

Oxygen isotope analyses were conducted on small batches of *Globigerinoides ruber*, the monospecific planktonic foraminifera that calcifies in the surface layer: 143 samples were collected in 1 cm thick sediment intervals, selecting intervals of continuous sedimentation and excluding reworked material (as turbidites). Cores were sub-sampled with a sample spacing of 5 to 20 cm. On average, three specimens were picked out from the >150 mm fraction and analysed using a KIEL isotope ratio mass spectrometer (Thermo Fisher Scientific, Waltham, MA, USA) at IUEM (Brest). The variations in $\delta^{18}\text{O}$ obtained along the sediment core are correlated with the LR04 world reference curve issued from benthic foraminifera (Lisiecki & Raymo, 2005). With this curve correlation, it is generally possible to distinguish the isotopic stages of the Quaternary and to calibrate its fluctuations over several hundreds of thousands years.

Strontium isotope stratigraphy (SIS) is a chemical stratigraphy tool well-established since the 1980s (Elderfield, 1986; McArthur, 1994). The method relies on the facts that: (i) Sr incorporated into carbonate structure (substituting Ca atoms) will have the same Sr-isotope composition (⁸⁷Sr/⁸⁶Sr ratios) as the fluid from which it precipitated; and (ii) the ⁸⁷Sr/⁸⁶Sr of Sr dissolved in the world's ocean has varied through time. ⁸⁷Sr/⁸⁶Sr ratios measured on carbonate samples can therefore be used to date and correlate marine carbonate worldwide. The arising difficulty with the SIS approach is to ensure that the measured ⁸⁷Sr/⁸⁶Sr ratio is representative of the original fluid composition. Indeed, diagenetic processes, secondary alteration of carbonate units by more recent seawater and/or meteoric fluids may modify the Sr-isotope composition of the

sample after deposition. The most seen effect is the impact of circulating recent seawater, which increases measured ⁸⁷Sr/⁸⁶Sr ratios. Indeed, the ⁸⁷Sr/⁸⁶Sr ratio of seawater has mostly increased since the last *ca* 100 Myr. Therefore, contamination by this recent fluid will tend to artificially increase the measured ⁸⁷Sr/⁸⁶Sr ratio.

Samples were measured at the PSO (Pôle de Spectrométrie Océan) in Brest, France. The 'Age to isotope composition' LOWESS 5 abacuses of McArthur (1994) were used to establish the relationship between the Sr-isotope compositions of shells and the age of the sediment deposition. This database allows the most precise SIS age determination at present day. From the ⁸⁷Sr/⁸⁶Sr ratio, chosen to represent the composition of the precipitating seawater, ages are determined using the abacuses and results state mean calculated ages together with upper and lower limits. Results for the seven samples used in this study are presented in Table 4.

RESULTS

This study focuses on the northern end of the Mozambique ridge (see location in Fig. 1) at 25°S and 36°30'E in the Limpopo corridor, between 1800 m and 2200 m of water depth. It is a first characterization of the submarine morphology and the internal structure of this sedimentary ridge. The results of sedimentological and stratigraphic analyses are then presented in order to analyse the recent evolution of the sedimentary ridge (deposits, processes, stratigraphy).

Morphology and sedimentary structure of the contourite drift

Morphology of the sedimentary ridge

The sea floor morphology is marked by a bathymetric high of about 400 m in height forming the main morphological ridge. It is NNE–SSW

Table 4. Strontium ages obtained on bulk carbonate sediment sampled in hemipelagic layers, measured by SEDI-SOR (Brest).

Core and section number	Sample (cm)	$^{87}\text{Sr}/^{86}\text{Sr}$	1 σ error	Age (Ma)	+/- (Ma)	Minimum $^{87}\text{Sr}/^{86}\text{Sr}$	Age max	+/- (Ma)	Maximum $^{87}\text{Sr}/^{86}\text{Sr}$	Age min	+/- (Ma)
MOZ3-CS05 S1	5–6	0.709007	0.000002	5.77	0.06	0.709005	5.80	0.06	0.709009	5.73	0.05
			>	5.71	0.06	>	5.75	0.05	>	5.68	0.05
			<	5.82	0.05	<	5.86	0.06	<	5.78	0.05
MOZ3-CS05 S4	316–317	0.709128	0.000003	1.160	0.04	0.709125	1.205	0.04	0.709131	1.116	0.04
			>	1.121	0.04	>	1.165	0.04	>	1.078	0.04
			<	1.201	0.04	<	1.242	0.04	<	1.156	0.04
MOZ3-CS05 S7	633–634	0.708998	0.000002	5.93	0.04	0.708996	5.96	0.04	0.709000	5.90	0.05
			>	5.89	0.04	>	5.92	0.04	>	5.85	0.05
			<	5.97	0.04	<	6.00	0.04	<	5.94	0.04
MOZ3-CS06 S1	5–6	0.709147	0.000002	0.797	0.05	0.709145	0.844	0.06	0.709149	0.751	0.05
			>	0.748	0.05	>	0.791	0.05	>	0.705	0.05
			<	0.852	0.05	<	0.907	0.06	<	0.803	0.05
MOZ3-CS06 S8	782–783	0.709225	0.000002	<i>Present Seawater</i>							
MOZ3-CS07 S7	600–601	0.709082	0.000002	2.12	0.10	0.709080	2.18	0.09	0.709084	2.05	0.10
			>	2.02	0.10	>	2.08	0.10	>	1.94	0.11
			<	2.21	0.09	<	2.26	0.08	<	2.15	0.10
MOZ3-CS07 S12	1100–1101	0.709044	0.000002	4.70	0.12	0.709042	4.78	0.10	0.709046	4.60	0.14
			>	4.56	0.14	>	4.67	0.11	>	4.44	0.16
			<	4.80	0.10	<	4.87	0.09	<	4.73	0.13

elongated, 75 km long and 50 km wide (Fig. 2). Two main channels are visible along the eastern and western edges of the ridge. They run parallel to isobaths and merge to the south. The eastern channel has a stronger incision at more than 2400 m of water depth. The western channel is between 2100 m and 2200 m water depth with a gentle slope to the north. The ridge is divided into two bathymetric highs, separated by a central erosional corridor (Fig. 2). Secondary elongated erosional features are visible near the top of the bathymetric highs. They look like small discontinuous channelizations. Due to the lack of continuity of high-resolution bathymetric data, it is difficult to identify sedimentary patterns that would unambiguously indicate current direction in the main channels.

The morphology of the central erosional area, which is open towards the north-east and closed at its south-western end, suggests that the flow forming this erosional area is from the south-west to the north-east (Fig. 2). Furthermore, the northern and southern ends of the ridge, are rounded and eroded, indicating a rotation of currents around this ridge (no clear sedimentary structures such as comet-tail type are visible as in the case of the main unidirectional current).

Seismic structure of the sedimentary ridge

The regional multichannel seismic profile, running dip to the Mozambique margin across the Limpopo Corridor (Fig. 3), shows the large-scale and deep structure of the sedimentary ridge. On the entire profile (Fig. 3A), the main regional stratigraphic reflectors were picked and tied to a well, located 3 km updip. This first interpretation was carried out and provided by the industrial partner TotalEnergies.

A detailed line-drawing is provided for a ‘zoomed-in’ image of the profile on the ridge (Fig. 3B and C). Seven seismic units were defined, from the older SU 1 to the most recent SU 7. The boundaries between the seismic units are stratigraphic surfaces that mark major changes in the evolution of the sedimentary series (geometrical changes of the sedimentary fill or erosional surface). The reflectors marked in red (Fig. 3C) are the stratigraphic markers identified on the entire profile (Fig. 3A). They represent most of the boundaries between the seismic units, except the Cretaceous–Tertiary boundary, which is located in the middle of the SU 3 seismic unit and the limit between SU 6 and SU 7, which correspond to a major change in the most recent sedimentary filling.

The base of the Cretaceous sedimentary succession (SU 1) is set on a major discontinuity with irregular geometry, marked by steep escarpments forming the base of the slope. The SU 1 seismic unit has a fan-shaped structure, with a strong thickening at the base of the escarpment. The seismic unit SU 2 is located above SU 1 but covers only its deeper part. The reflectors are parallel but the unit is slightly thicker at mid-profile and shows an internal erosion surface. The top reflector is erosive in its western part. The seismic unit SU 3 is a 1 s TWT thick unit in its thickest part, which overlaps SU 1 and SU 2. At the base of the escarpment (north-west side), this seismic unit contains numerous erosional surfaces suggesting a succession of channelization over a width of about 15 km. The erosional surfaces extend into a thick succession of parallel, continuous and concordant reflectors inside the ridge, suggesting strong sedimentary aggradation. The reflectors are linear and regular at the base of SU 3 and become jagged and wavy at the top of the unit. The upper limit of unit SU 3 is an erosional surface in the channelized area and on the eastern side of the ridge.

Seismic unit SU 4 is located between two major erosional surfaces. The reflectors within this unit are concordant and parallel and follow the slopes and irregularities of the basal erosional surface. On the upper part of the escarpment, it extends towards the upper slope to the north-west. As for the SU 3 unit, the reflectors are continuous and smooth at the base of SU 4 and become jagged and wavy at the top of the unit, especially on the ridge. The top of this SU 4 unit is strongly eroded and incised by multiple channels. The only uneroded area is the top of the ridge. Seismic unit SU 5 shows numerous erosional surfaces, especially in the western part of the profile where this unit has a sediment thickness of 0.5 s TWT. The reflectors are concordant and parallel on the top of the ridge, which narrows upward. On the western flank of the ridge, the geometry of the reflectors is variable with lens-shaped deposits, draping shapes and local erosions. The top of unit SU 5 is an erosional surface that cuts a deep (>1 s TWT) and 5 to 10 km wide channel parallel to the slope, between the upper slope and the ridge.

The last two seismic units SU 6 and SU 7 are two filling units of the deep incision at the base of SU 6. The reflectors are in onlap on the basal erosional surface. The SU 6 seismic unit firstly fills the channel bottom and then covers the western side of the channel with oblique

reflectors. Seismic unit SU 7 is the last unit of the channel infill. The internal reflectors are very irregular with many small incisions. The later reflectors have geometries that suggest cross-sections of small channel-levée systems.

Superficial sedimentary structures highlighted by the CHIRP sediment profiler

Despite the low penetration of the signal, the CHIRP profiles (Fig. 4) show irregular sediment coverage and erosional markers. On profile MOZ3-SDS-0038 (Fig. 4), the sedimentary layers are characterized by reflectors sub-parallel to the sea floor that extend mainly on the western flank of the ridge. They have a maximum thickness at the centre of the profile at the location of two small bathymetric highs. The layers thin to the east towards the top of the ridge. Around the top of the ridge, sub-horizontal reflectors are truncated by the sea floor, especially at the eastern flank of the ridge, which appears to be almost entirely affected by erosion (grey area in Fig. 4). Close-up views of this profile are provided in Fig. 5. On the two other CHIRP profiles (MOZ3-SDS-0053 and 0055 in Fig. 4) acquired across the southern high, the geometry of the reflectors is complex and irregular with concave and convex shapes. On the sides of the ridge, the reflectors are truncated by the sea floor, indicating present erosion (in grey in Fig. 4). Only the top of the ridge shows layers parallel to the sea floor indicating sedimentary drape (profile MOZ3-SDS-0053 in Fig. 4).

The detailed analysis of the MOZ3-SDS-0038 profile shows two main reflectors along the western flank of the ridge (orange and blue lines in Fig. 5). The continuity of these reflectors between the MOZ3-CS03 and MOZ3-CS02 core sites is interrupted with the relief, but the analogy of the succession of reflectors on zooms 1 and 2 of this profile (Fig. 5) indicates a possible correlation between the two cores. The orange and blue reflectors get very close and finally reach the sea floor surface eastward towards the MOZ3-CS07 core site, where the layers appear condensed (Fig. 5).

Sedimentological characterization of the Quaternary deposits

The five cores collected on the ridge are between 5 m and 20 m long (Table 1). Sedimentological logs of the five cores are presented in Fig. 6, in the order of their location from west to east. Figures 7 to 9 illustrate the sandy facies with

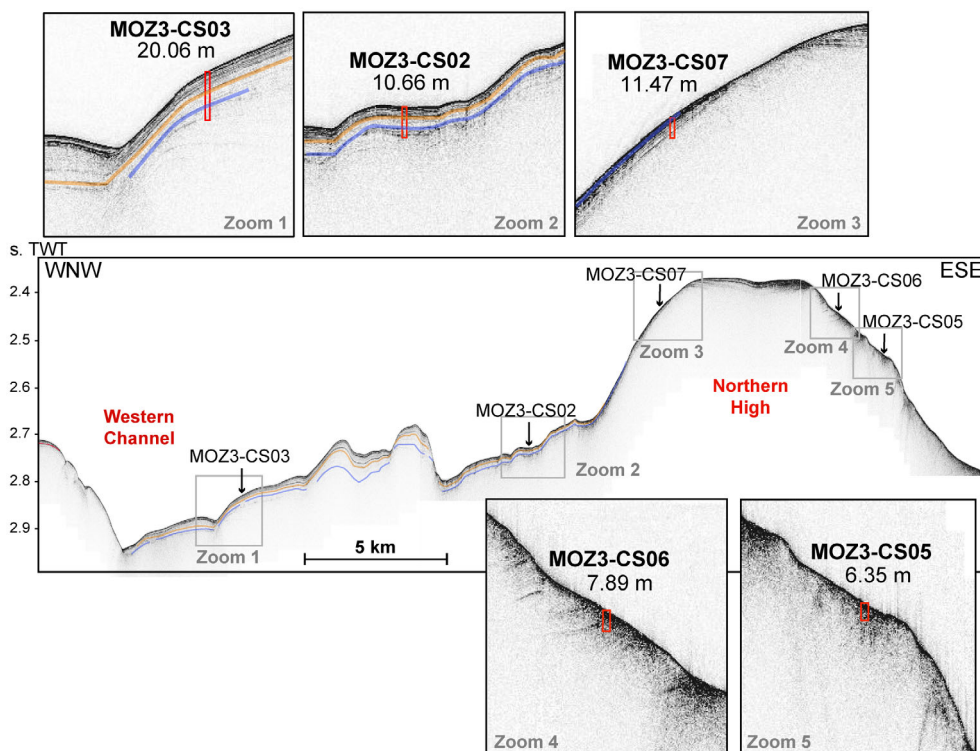


Fig. 5. CHIRP profile MOZ3-SDS-0038 with two reflectors (yellow and blue) and zooms of the profile nearby the location of the five cores (CHIRP profile without interpretation visible in Fig. 4).

photographs, X-ray images and grain-size spectra, and the results of the mineralogical compositions for cores MOZ3-CS03 (Fig. 7), CS02 (Fig. 8) and CS07 (Fig. 9). Microfacies are illustrated in Fig. 10.

The core MOZ3-CS03 is 20.06 m long (Table 1; Figs 2 and 5). It was acquired at a water depth of 2125 m. Sedimentary facies are; silty clay facies (light grey in Fig. 6) and sandy facies (yellow in Fig. 6). Sandy facies are characterized by very fine to medium sand layers with sharp base, normal grading to silt grain size at the top, horizontal laminations and occasionally oblique laminations suggesting current ripples. For two of the fine sandy layers, the basal contact is gradual. The silty-clay facies contain foraminifera and are generally affected by numerous bioturbations. The colour varies from grey to greenish, with light/dark alternating shades (upper part of Fig. 7A, zoom A). The mineralogical composition of sample s1 (Fig. 7B) and s12 (Fig. 8) shows that it is a carbonate mud with more than 50% of carbonate in composition. The clay content is about 30% for these samples and the proportion of detrital minerals such as quartz and feldspar is less than 20%. The two

sandy sequences of core MOZ3-CS03, presented in Fig. 7C, show multi-decimetres sandy deposits with an erosive base, normal grading and are intensively laminated. Between 1135 cm and 1140 cm (Fig. 7C, zoom A), wavy laminations suggest the presence of current ripples. The transition to muddy facies at the top of the sequence is gradual. The mineralogical composition of the sandy layer evolves vertically (Fig. 7C, zoom B), as grain size. At the base, the grain size corresponds to medium sand (>300 μm) and carbonates or bioclasts are dominant (>50% in s7, Fig. 7B) with a relatively low density (X-ray image). In the upper part of the sandy layer, detrital minerals are largely dominant with more than 65% on average (35% quartz and 30% feldspar in s6; Fig. 7B) with a finer grain size around 100 μm and a higher density.

The core MOZ3-CS02 is 10.66 m long and was collected at a water depth of 2041 m (Table 1; Figs 2 and 5). The silty-clay sedimentary facies is dominant along the upper 6 m of the core (Figs 6 and 8). The foraminifera content is high in these muddy facies. Three laminated layers of foraminiferous sand are present at the top of the

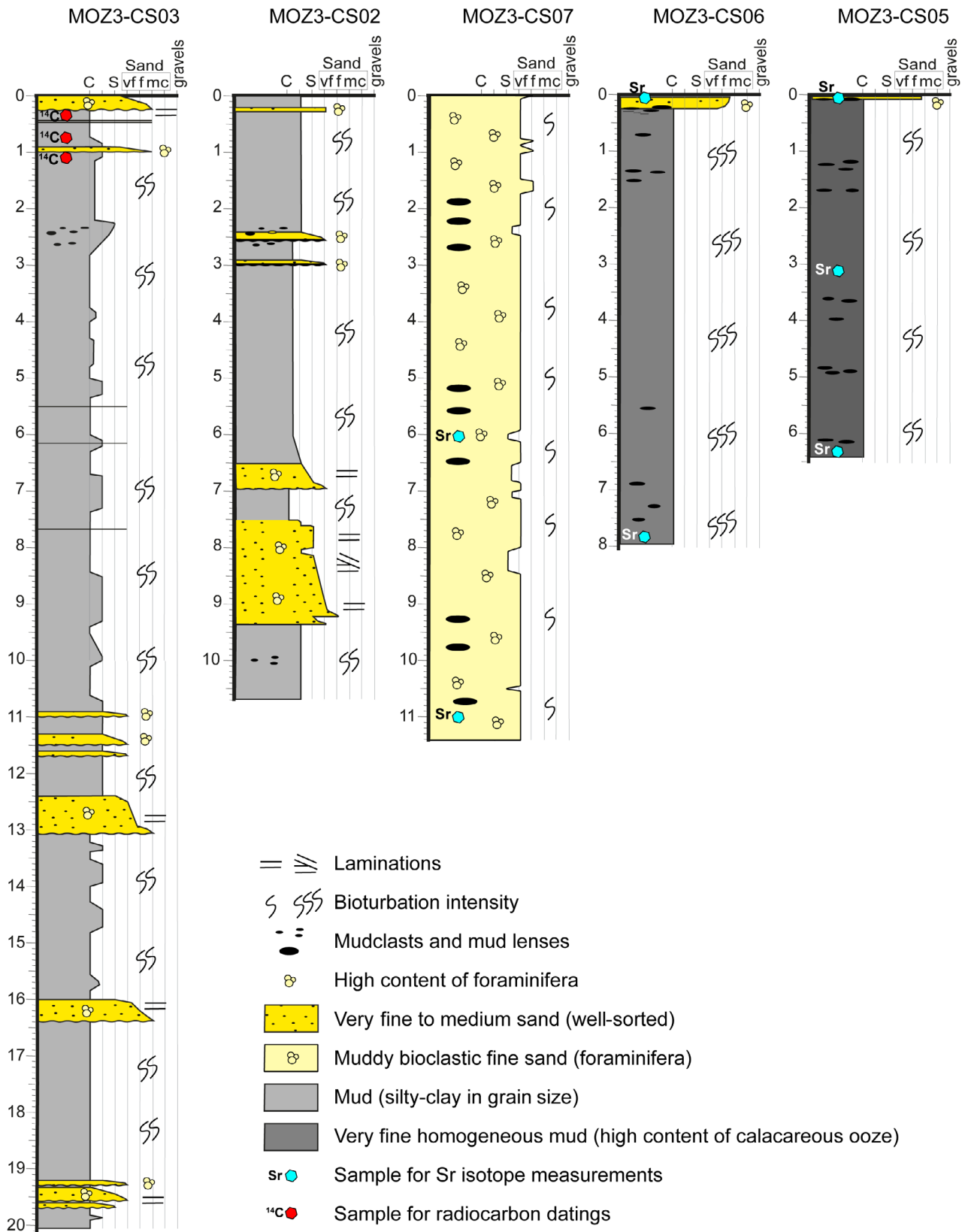


Fig. 6. Sedimentological logs of the five cores (vertical scale in metres).

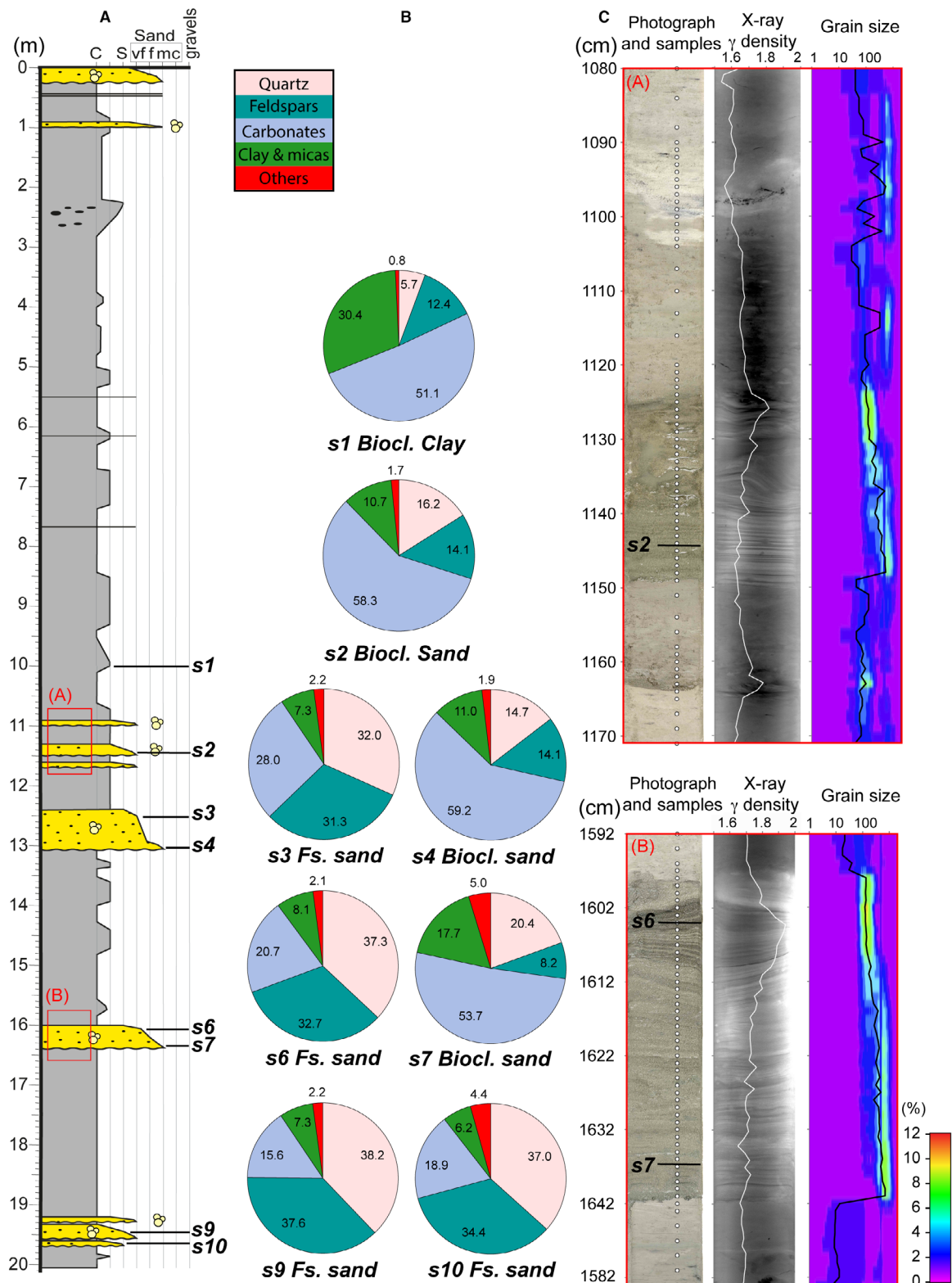


Fig. 7. (A) Sedimentological log of core MOZ3-CS03, (B) mineralogical composition by Qemscan® and BQM analysis (pie chart indicating quartz, feldspar, carbonate, clay, mica and other), and (C) two zooms of the core for the sedimentological characterization including photographs and sample locations for laser grain-size measurements, X-ray images and gamma-density curve, laser grain-size spectrums and D50 curve (between 2 µm and 2000 µm). *Biocl.* – bioclastic, *Fs.* – feldspar.

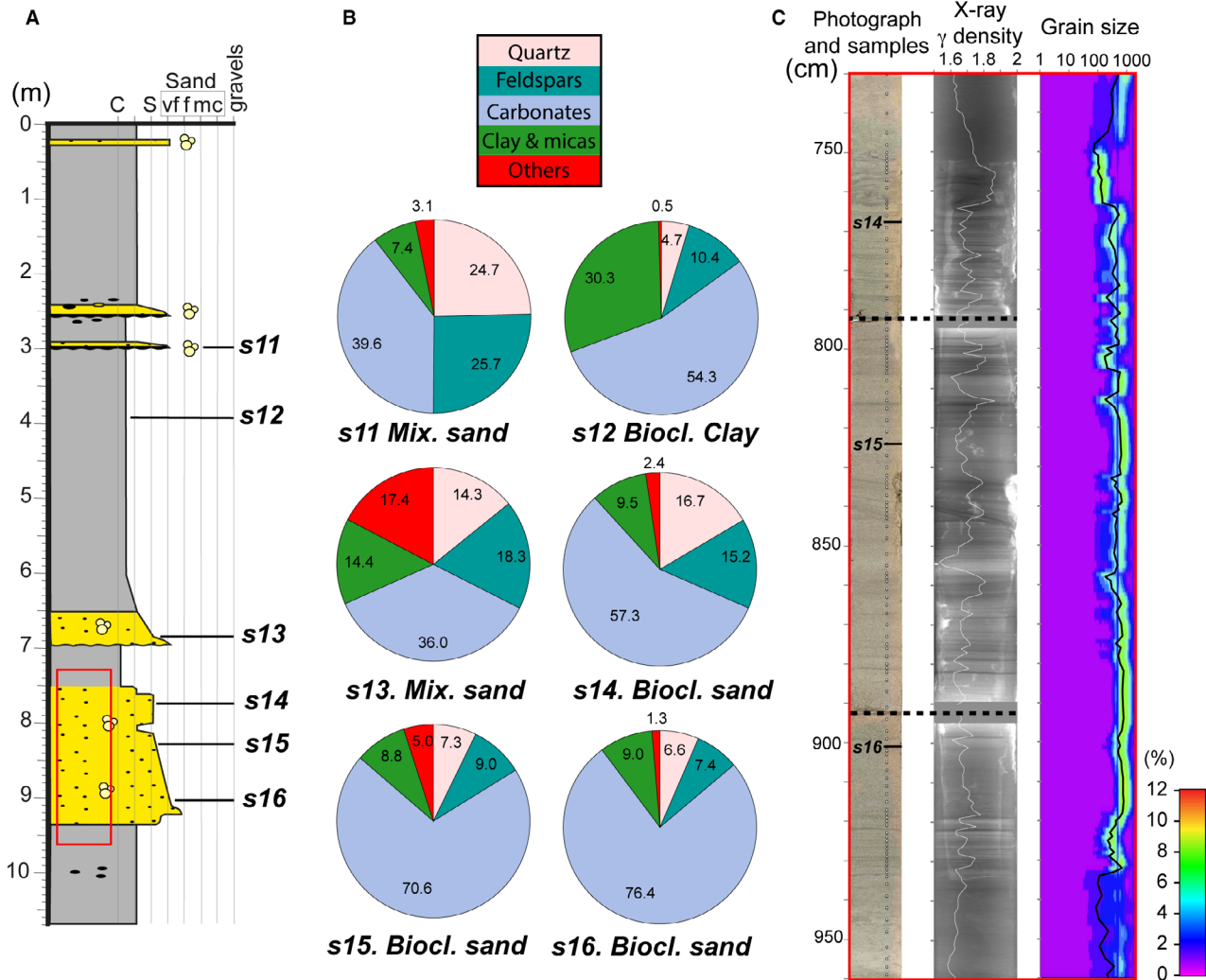


Fig. 8. (A) Sedimentological log of core MOZ3-CS02, (B) mineralogical composition by Qemscan® and BQM analysis (pie chart indicating quartz, feldspar, carbonate, clay, mica and other), and (C) one zoom of the core for the sedimentological characterization including photographs and sample locations for laser grain-size measurements, X-ray images and gamma-density curve, laser grain-size spectrums and D50 curve (between 2 µm and 2000 µm). *Biocl.* – bioclastitic, *Fs.* – feldspar.

core. These layers present a sharp base and normal grading. Between 932 cm and 750 cm in the core (Fig. 8), the sandy deposit is 1.82 cm thick, composed mainly of carbonates (70% bioclasts on average in s15 and s16, Fig. 8B) with a median grain size in coarse sand at 500 µm (Fig. 8C). Well-marked laminations are visible all the way along the deposit with a few oblique laminae around 840 cm (X-ray image, Fig. 8C). The base of the deposit shows a progressive transition with an inverse grading, followed by significant variations in grain size and in density throughout the thickness of the deposit (Fig. 8C). The top transition is also progressive with the

appearance of bioturbation and the gradual increase of mud content.

The microfacies analyses of sandy facies of cores MZ03-CS03 and MZ03-CS02 by Qemscan® and BQM methods show that feldspars (K-feldspar and plagioclase) are abundant, with locally 25% of feldspars (Figs 7, 8 and 10). Content of heavy minerals is significant, up to 5.7% with BQM analysis (underestimated by Qemscan® at ca 2%). Amphibole, apatite, pyrite, goethite and the group rutile/anatase/brookite are detected by Qemscan®. Bioclasts have a larger size than mineral grains (quartz and feldspar), often leading to bimodal grain-size

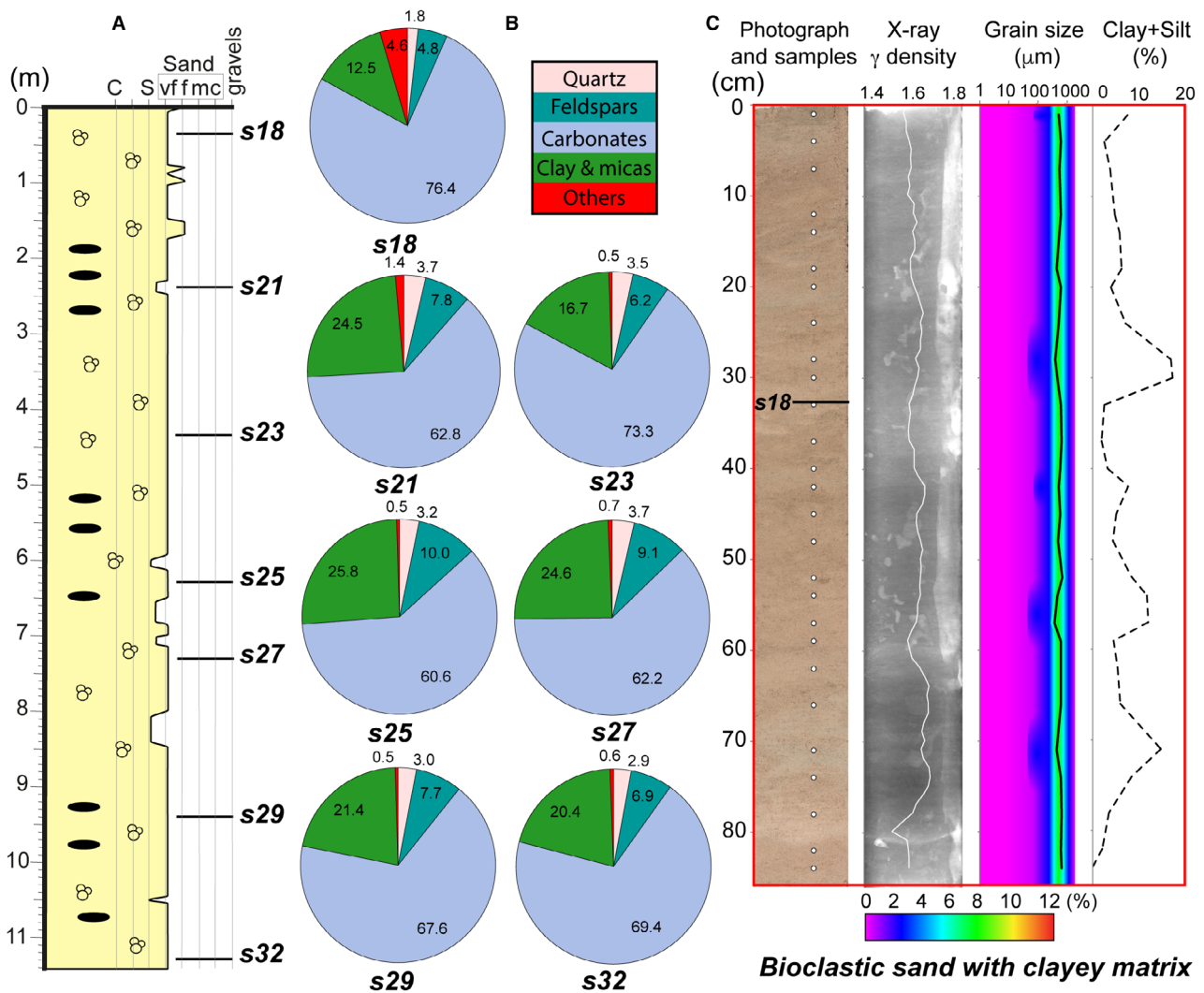


Fig. 9. (A) Sedimentological log of core MOZ3-CS07, (B) mineralogical composition by Qemscan[®] and BQM analysis (pie chart indicating quartz, feldspar, carbonate, clay, mica and other) and (C) one zoom of the core for sedimentological characterization including photographs and sample locations for laser grain-size measurements, X-ray images and gamma-density curve, laser grain-size spectrums and D50 curve (between 2 μm and 2000 μm), fine-grained sediment content (silt + clay grain size in %).

frequency plots (Fig. 10). Signs of reworking are visible with lithified sandstone lithoclasts found within bioclastic sand or lithified calcarenite lithoclasts found within detrital sand. Heterogeneous texture possibly results from bioturbation.

The core MOZ3-CS07 is located at the top of the western flank of the ridge. Collected at a water depth of 1853 m, its length is 11.47 m (Table 1; Figs 2 and 5). It is composed of bioturbated foraminiferous sand (Figs 6 and 9). The grain size is directly related to the size of foraminifera (Fig. 6), while the matrix is made of silt, or even silty-clay. The core is entirely sandy in terms of grain size with an average median in

coarse sand at 575 μm (coarse sand), as illustrated along the upper section (Fig. 9). The sediment is composed mainly of foraminifera tests (bioclastic sand). Microfacies observation and mineralogical analysis reveal the occurrence of clayey to silty matrix. This facies does not correspond to clean sands. It can be considered as a foraminifera calcarenite with a muddy matrix (12 to 26% of clays and 6 to 12% of detrital grains; see pie-charts of Fig. 9B). Visual observation of the core, X-ray image and muddy content (clay and silt) clearly show distinct layers with vertical variations (Fig. 9C): high-density layers, rich in fine-grained sediment

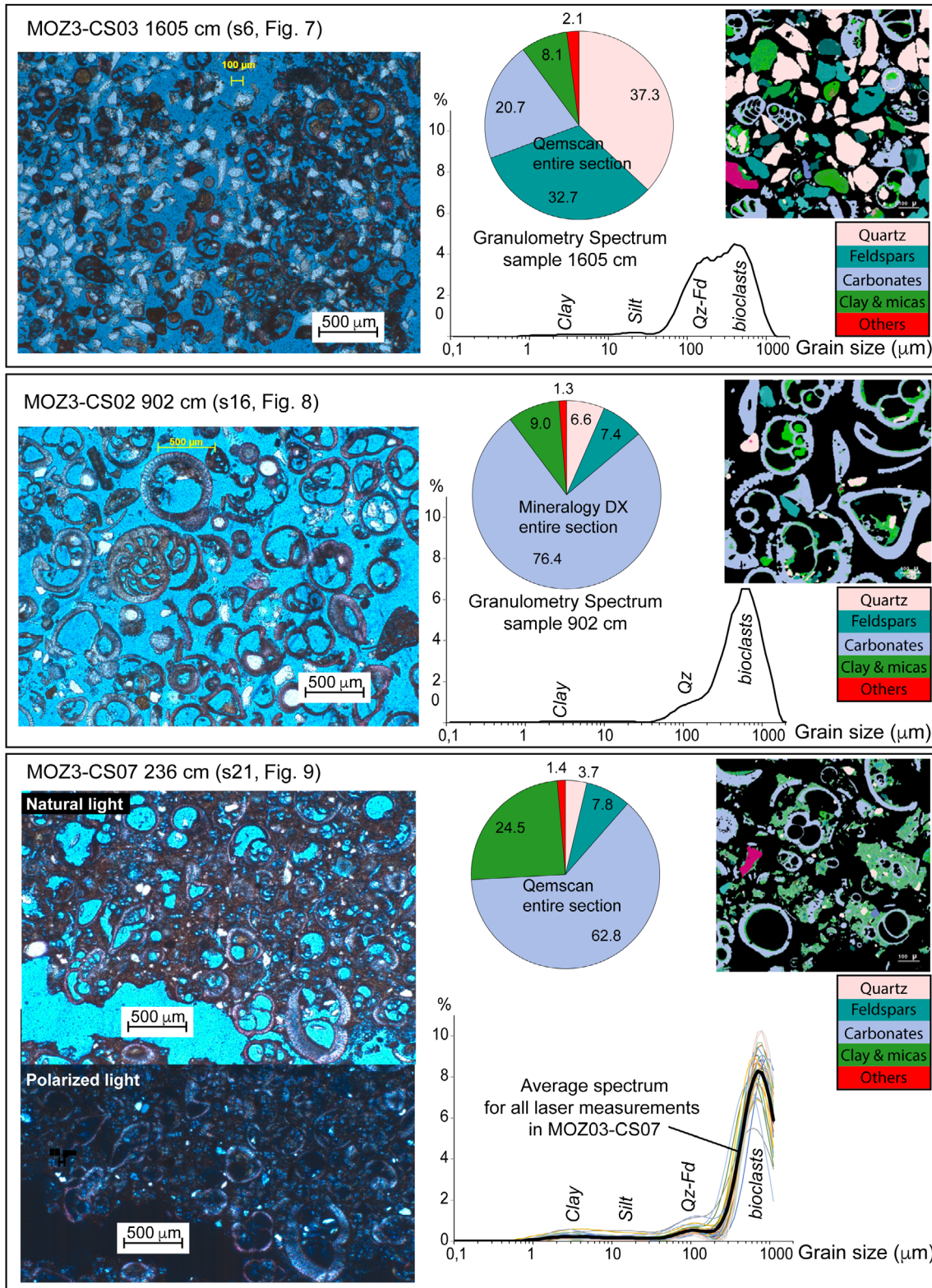


Fig. 10. Microfacies characterization including smear slices photographs, Qemscan® images and mineralogy pie charts, and laser grain-size spectra for the following three samples. (A) Core MOZ3-CS03, sample at 1605 cm. (B) Core MOZ3-CS02, sample at 902 cm. (C) Core MOZ3-CS07, sample at 236 cm.

alternate with low-density layers with low fine-grained sediment content (less than 5%).

The core MOZ3-CS06 was collected from the upper part of the eastern side of the ridge (Figs 2 and 5). It is 7.89 m long and was collected at a water depth of 1868 m. Core MOZ3-CS06 shows a sandy layer at its top with a thickness of 20 cm of fine to medium foraminiferous sand, characterized by a reverse grading (Fig. 6). Black spots of organic matter underline the base of this sandy layer. The rest of the core is homogeneous with carbonate mud (clay grain size) containing few foraminifera. It is highly bioturbated, with alternating brown, greyish and pinkish levels.

The core MOZ3-CS05 is located on the eastern side of the northern segment of the ridge, slightly downslope of CS06 (Figs 2 and 5). It is 6.35 m long and was collected at a water depth of 1926 m. The top of the core shows 2 cm of fine to medium foraminiferous sand (Fig. 6), with some black spots of organic matter. The rest of the core is homogeneous and shows a succession of greyish, ochre-brown and pink carbonate mud (clay grain size), generally bioturbated with few foraminifera.

Stratigraphy, age models and sedimentation rates

In this study, the stratigraphy of the cores is obtained using radiocarbon and Sr-isotope dating, isotopic stratigraphy ($\delta^{18}\text{O}$) and core correlation (see *Data and methods* section). The stratigraphical range of the MOZ3 cores is modern (at sea floor), Quaternary and Late Tertiary.

Radiocarbon dating and isotopic stratigraphy of core MOZ3-CS03

The three radiocarbon dates on planktonic foraminifera (*Globigerinoides ruber*) taken in pelagic intervals are consistent (see Table 3) and give a low sedimentation rate of 1.37 cm/ka calculated between the first two sampling points. The first date is about 7 ka cal BP at 35 cm; but because the first 25 cm of the core represent a sand layer suspected to be related to creeping during coring, the 7 ka date would be approximately 10 cm below the sea floor (taken by the core). This provides a sedimentation rate of about 1.4 cm/ka on the surface layer (consistent with the rate calculated below).

Figure 11 shows the most significant physical and chemical curves acquired along the MOZ3-CS03 core: lightness (L^*), magnetic susceptibility,

chemical element ratios Ca/Fe and Zr/Rb represented with log scale and $\delta^{18}\text{O}$ values acquired on the shells of planktonic foraminifera (*Globigerinoides ruber*). $\delta^{18}\text{O}$ sampling was not carried out in the sandy layers (suspicion of sediment reworking), resulting in a discontinuous curve, especially over the lower half. Variations of lightness (L^*) and $\log(\text{Ca/Fe})$ curves are anticorrelated. The $\log(\text{Zr/Rb})$ curve also shows cycles of the same wavelength but with various amplitudes. The magnetic susceptibility signal has a different vertical evolution and follows variations of sedimentary facies with the addition of two peaks at the top of the core and a series of peaks between 8 m and 11 m depth.

The $\delta^{18}\text{O}$ variations have steady amplitude with large cycles from 50 cm to 1 m thick in wavelength. The fitting of the upper half of the $\delta^{18}\text{O}$ curve with the reference curve LR04 (Fig. 11) is obvious until Marine Isotope Stage 15. The correlation of the lower half is less robust because the $\delta^{18}\text{O}$ signal is not continuous and the isotopic stages less well-expressed. However, it is probable that the base of the core exceeds 1 to 1.15 Ma. The maximum sedimentation rate, estimated by the O-isotope curve, is about 1.7 cm/ka over the entire core. The four thickest sandy layers are estimated at about 650 ka, 750 ka, 900 to 950 ka and 1100 to 1150 ka, respectively.

The cycles described on the physical and chemical parameters [curves of L^* , $\log(\text{Ca/Fe})$ and $\log(\text{Zr/Rb})$] correlate approximately with the climatic cycles identified on the $\delta^{18}\text{O}$ curve. This correlation is not perfect but the variability is consistent with a control from the global insolation cycles (20 ka and 40 ka cycles) and eccentricity cycles (100 ka).

Strontium dating on MOZ3-CS05, MOZ3-CS06 and MOZ3-CS07

Measurements of Sr-isotopes were carried out on the sediments that were estimated to be the oldest, in particular through the analysis of CHIRP profiles indicating sea floor erosion or condensation of deposits (see location of Sr measurements in Fig. 6). Sediments of the MOZ3-CS05 core cover a time interval between 5.68 Ma (minimum value at 5 to 6 cm below the sea floor) and 6 Ma (maximum value at 633 to 634 cm below the sea floor), with an average sedimentation of 3.9 cm/ka between the two measured samples. The measurement at 316 to 317 cm below the sea floor provides a low value, which was estimated to be incorrect (Table 4)

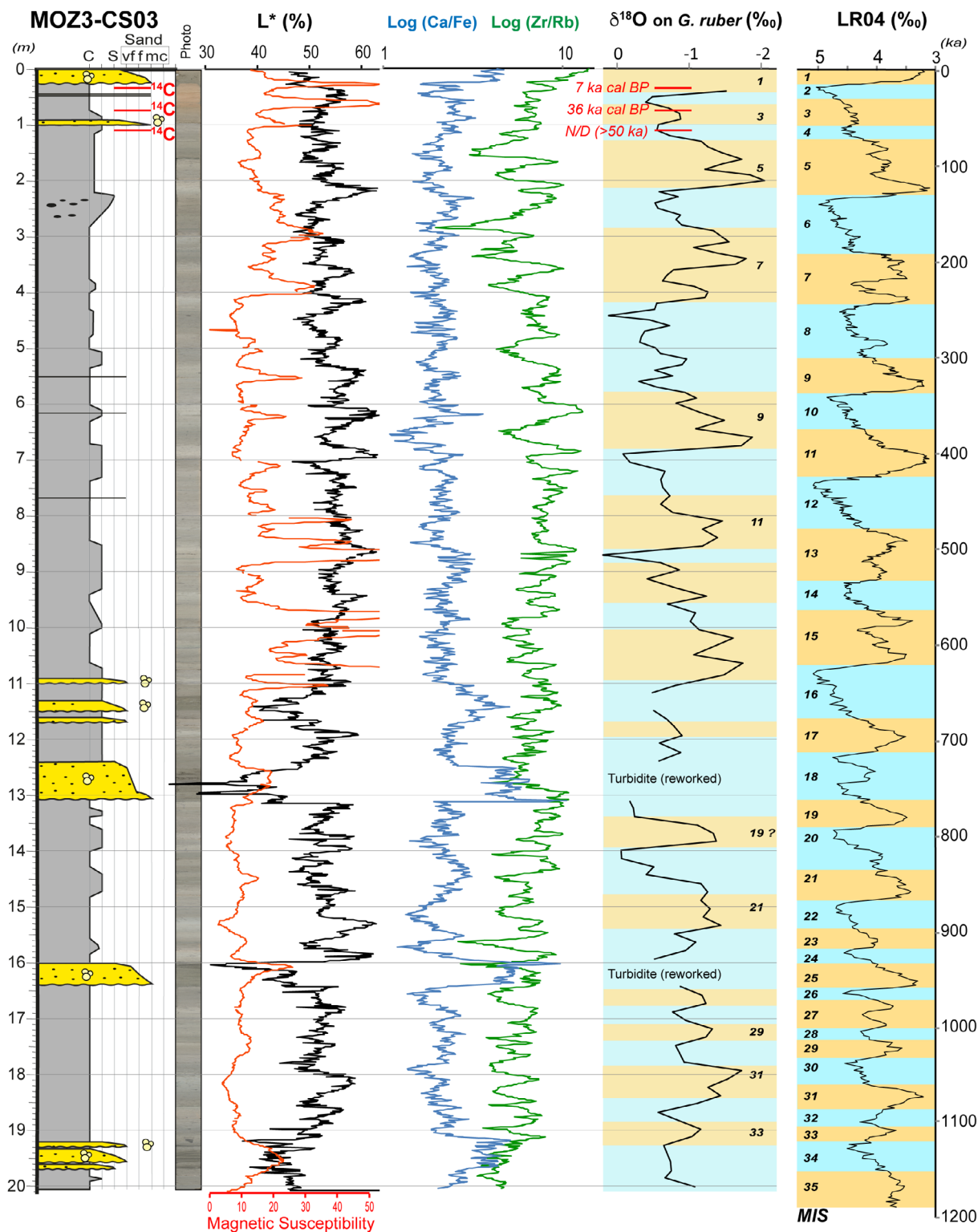


Fig. 11. Sedimentological log of core MOZ3-CS03, photographs, curves of lightness L^* in black, magnetic susceptibility in red, curves of chemical ratio acquired with the XRF core-scanner $\log(\text{Ca/Fe})$ in blue and $\log(\text{Zr/Rb})$ in green, curve of $\delta^{18}\text{O}$ measured on planktonic foraminifera (*Globigenoides ruber*) and hypothetical correlation of isotopic stage (MIS) established in comparison with the reference curves of $\delta^{18}\text{O}$ LR04 (Lisiecki & Raymo, 2005).

due to probable contamination. This problem of contamination is frequent on the bulk sediment, where carbonate separation was not possible in carbonate mud. It is difficult to envisage this value being correct, given the consistent age range of the other two Sr measurements on the same core and also a homogeneous facies (also in agreement with the observation of significant sea floor erosion on the seismic and CHIRP profiles).

For the MOZ3-CS06 core, the top sample was taken 5 cm from the top sandy unit above the erosion surface. It is probably a condensed sandy deposit since the age at 5 cm is measured between 0.7 Ma and 0.9 Ma (Table 4). The measurement taken on the sample at 782 to 783 cm has a present-day seawater value, probably also due to contamination. The sediments in the MOZ3-CS06 core are younger than those in the MOZ3-CS05 core. Based on their stratigraphic position on the flank of the ridge (Fig. 5), they probably are in the range from 1 Ma to 3 Ma.

Finally, two Sr-isotope measurements were performed on samples from the MOZ3-CS07 core (location in Fig. 9). These two values are consistent in terms of stratigraphy and indicate an age of about 2.05 to 2.26 Ma at 6 m below the sea floor and 4.6 to 4.87 Ma at 11 m below the sea floor. The sedimentation rate between these two samples is therefore as low as 0.2 cm/ka. If the upper part of the core corresponds to continuous sedimentation until present-day, as indicated by the apparent continuity of the sedimentary facies, the average sedimentation rate for the upper part is 0.28 cm/ka. Because of these extremely low rates, the sedimentation of this core can be considered as condensed sedimentation.

Correlation between cores MOZ3-CS03, MOZ3-CS02 and MOZ3-CS07

The correlation between the three cores is based on two approaches: (i) the interpretation of the CHIRP profile, on which the three cores are located (profile MOZ3-SDS-0038); and (ii) the correlation of the physical and chemical profiles of the cores (MSCL and XRF data) identifying consistent variations and cycles caused by external forcing. For clarity of interpretation, only the two log curves of the Ca/Fe and Zr/Rb ratios illustrate these correlations in Fig. 12. These two curves show the most significant variations allowing the correlations of the three cores.

Because of the variations in sedimentary facies (from one core to another and vertically within the same core), the correlation is not perfect in detail, but consistent with the stratigraphy of large depositional sequences (colour bands in Fig. 12). No major interruption is observed in the sediment succession, indicating consistency and continuous sedimentation along the three cores, despite different sedimentation rates. Indeed, the sedimentary succession is two times more condensed in the MOZ3-CS02 core than in the MOZ3-CS03 core and about ten times more condensed in the MOZ3-CS07 core than in the MOZ3-CS03 core.

The sandy deposits described in the MOZ3-CS03 and MOZ3-CS02 cores are correlated (dotted lines in Fig. 12), despite lateral variations in facies, thickness and layer sequencing. The yellow interval (Fig. 12) between 12.5 m and 16.5 m in the MOZ3-CS03 core shows two sandy layers at the base and top. It correlates directly with the thickest sand layer of the MOZ3-CS02 core between 7.5 m and 9.5 m below sea floor.

DISCUSSION

The morphology of the Mozambique sedimentary ridge (bathymetry in Fig. 2) is marked by the two longitudinal channels on either side of the ridge and along the continental margin. The north–south elongated shape of the ridge perpendicular to the continental margin slope is clearly linked to bottom current circulation along the margin between 1800 m and 2200 m depth. The relief formed by sediment accumulation corresponds to a contourite drift, and the western channel corresponds to the moat. According to the interpretation of the seismic profile, the current morphology of this contourite system and the recent sedimentary evolution of the ridge are probably different from those of the past construction stages. Based on the data presented in the previous section, the discussion focuses first on the sedimentary structure of the ridge to briefly discuss the different stages of formation and evolution of this sedimentary ridge. The discussion then addresses the sedimentary facies and Quaternary processes occurring on the Mozambique sedimentary ridge, which is the major contribution provided by the coring data. The distribution of coarse-grained contouritic facies is also considered. Finally, the interpretation of the recent morphology and processes is

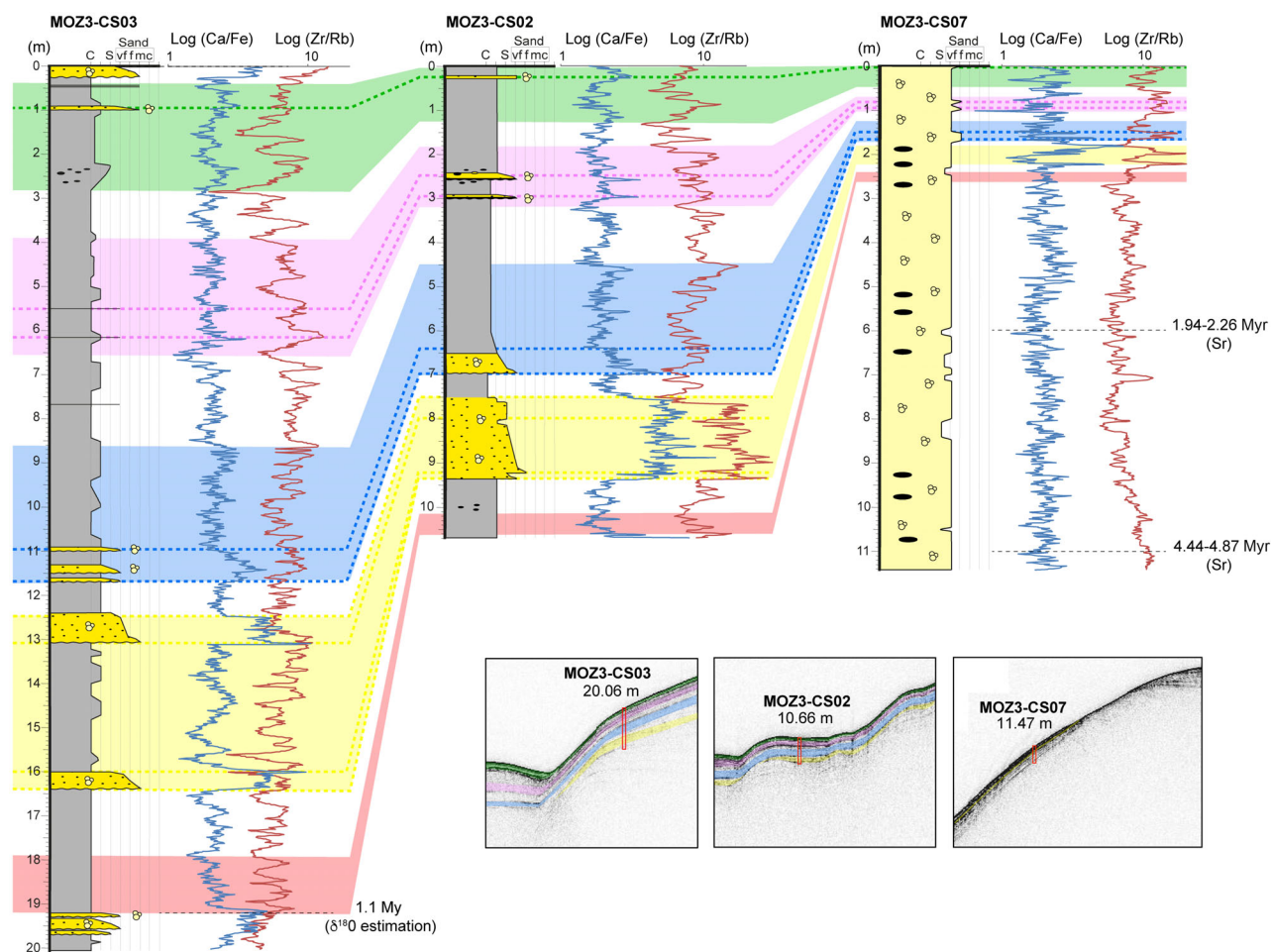


Fig. 12. Proposed stratigraphic correlation between the three cores MOZ3-CS03, MOZ3-CS02 and MOZ3-CS07 based on the isotopic stratigraphy of MOZ3-CS03 ($\delta^{18}\text{O}$), Sr dating of MOZ3-CS07 and chemical ratio $\log(\text{Ca}/\text{Fe})$ and $\log(\text{Zr}/\text{Rb})$ obtained by core-scanner measurements. Bottom right shows the three zooms of the CHIRP profile passing through the three core points (shown in Fig. 5), with the coloured band used for correlation of the cores.

discussed in the context of present and Quaternary ocean circulation.

Formation and evolution stages of the sedimentary ridge

The interpretation of the seismic profile across the sedimentary ridge (Fig. 3) allows to distinguish three stages in the ridge formation and evolution (Fig. 13). After the sedimentation of a fan-like shape at the base of the slope (seismic unit SU 1) during the Early Cretaceous, the ridge formation is initiated with the deposition of the seismic units SU 2 and SU 3, during the Late Cretaceous, Palaeocene and Eocene (Stage 1, Fig. 13). The thick sediment accumulation at the location of the ridge and the successive erosion

at the base of the escarpment show the initiation and development of the typical contourite system with aggradation on the drift and the contemporaneous incision of the moat.

Stage 2 (Fig. 13) corresponds to the deposition of the seismic units SU 4 and SU 5, during the Oligocene and the Miocene. During this stage, the contourite drift was still aggrading but the aggradation slowed down. The base of the Miocene is marked by a surface of deep incisions on the upper slope with channelized forms, and a deepening and widening of the moat. During the Miocene, the sedimentary succession is marked by several phases of incision (moat and upper-slope) alternating with aggradation.

Stage 3 (Fig. 13) corresponds to the deposition of the seismic units SU 6 and SU 7, during the

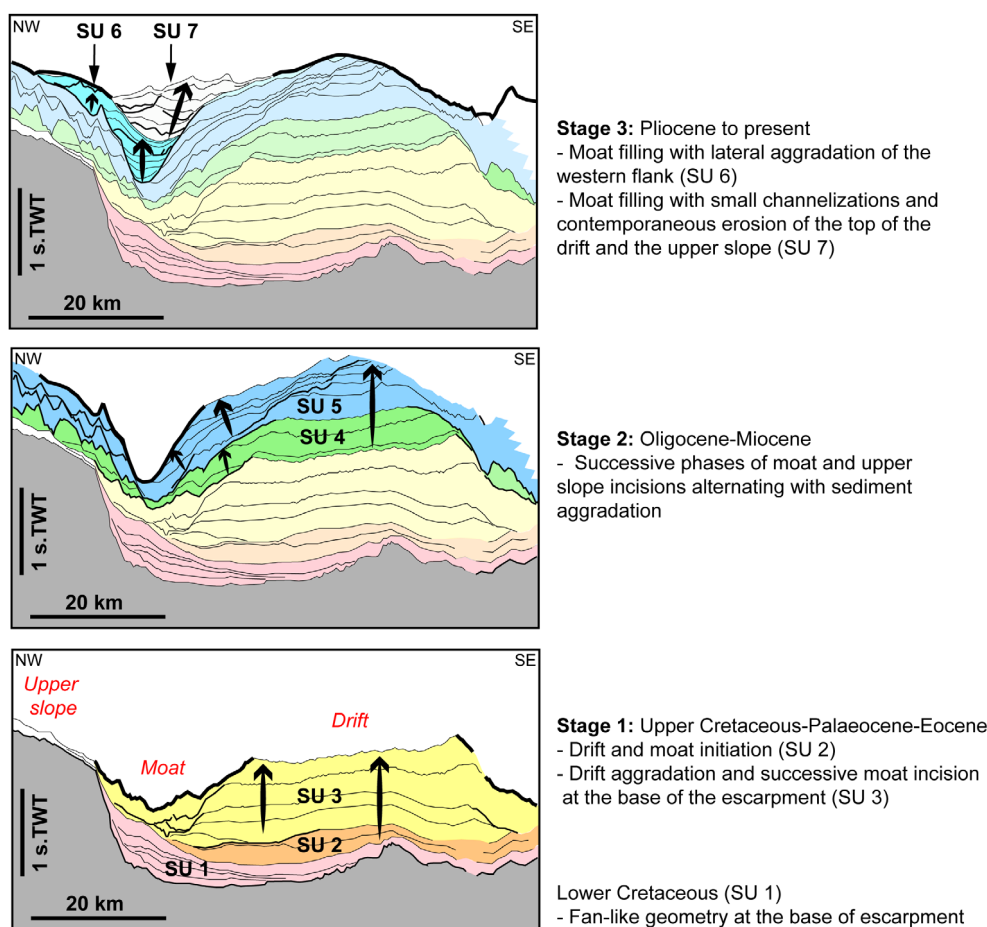


Fig. 13. Sketch of the main evolution stages of the sedimentary ridge (coloured areas and SU for seismic units, bold lines for erosional surfaces).

Plio-Quaternary. The base of the Pliocene is marked by a deep (about 1 s TWT) vertical incision of the moat. Plio-Quaternary sedimentation is characterized by a two-phase filling of the moat. The last unit (SU 7) constitutes the almost complete infill of the moat with sedimentary layers including numerous erosional surfaces. These erosion and deposition shapes suggest channel-levée systems, whereas the upper slope and the top of the ridge are in erosion.

The area of high current velocity has migrated laterally over time. This migration is probably due to a modification of the deep currents and the general oceanographic circulation but also partly to the morphological evolution of the ridge itself.

The sedimentary ridge shows three stages of evolution of the contourite system as described by Thiéblemont *et al.* (2020) on the northern part of the Mozambique margin with: (i) drift growth stage until the Oligocene; then (ii)

slowing down of growth with several stages of erosion and stability until the Miocene; and, finally, (iii) a moat-filling stage until the present. In the paper of Thiéblemont *et al.* (2020), the moat filling stage is interpreted as resulting from the onset of the NADW and the AAIW from the Miocene, which significantly changes the water circulation along the Mozambique margin.

Stratigraphic record and sedimentary processes

The eastern flank of the sedimentary ridge shows erosion (Fig. 14) at all scales with truncated reflectors in the seismic profile (Fig. 3) and in CHIRP profiles (Figs 4 and 5). In both cores MOZ3-CS05 and MOZ3-CS06, the top is marked by a superficial sandy layer (respectively 2 cm and 20 cm thick), mainly composed of foraminifera, overlying in unconformity the

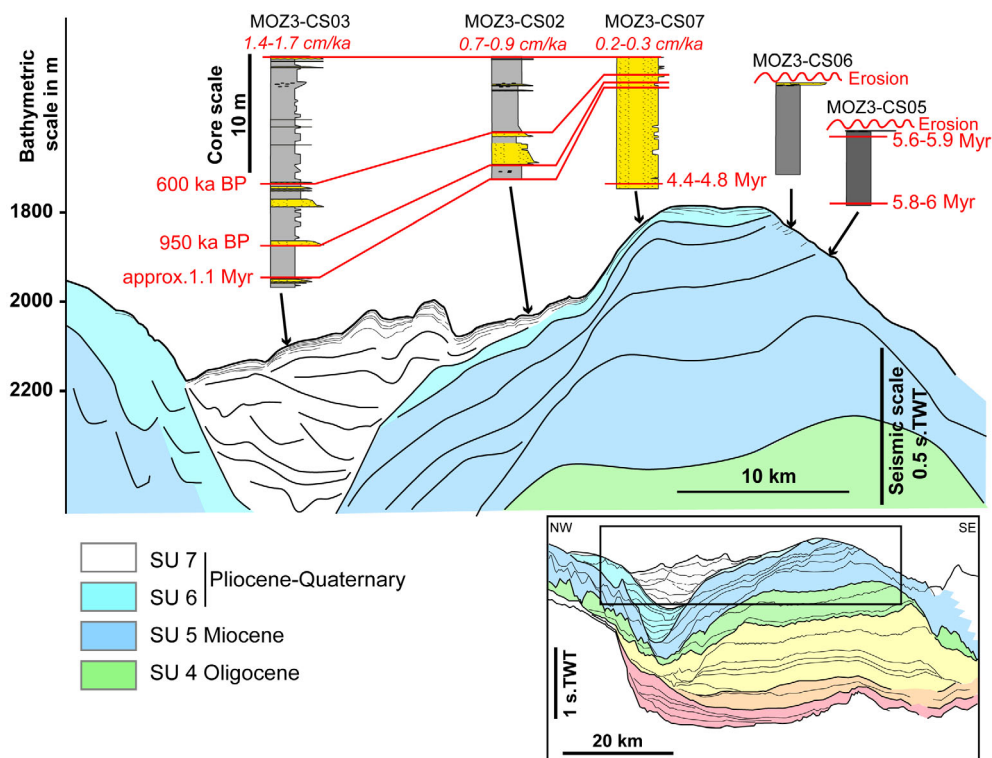


Fig. 14. Synthesis of stratigraphic data, consistency between seismic data, CHIRP data and cores (different scales for core logs, bathymetric profile and seismic units), harmonized to the location of the CHIRP profile MOZ3-SDS-0038 in Fig. 5, and the regional seismic profile MZ-05 in Fig. 1 (same line location).

homogeneous indurated calcareous mud. Although there are no convincing Sr-isotope results on core MOZ3-CS06, Sr-isotope measurements on core MOZ3-CS05 (top and bottom of the core) give consistent results between 5.6 Myr and 6 Myr, showing that the clay accumulations collected in these two cores are of Miocene age (Fig. 14). This result is consistent with the stratigraphic results deduced from the interpretation of the seismic profile. The superficial foraminiferal sands probably correspond to condensed sedimentation above the erosion surface. At 5 to 6 cm below the surface, a dating between 700 ka and 900 ka is given by Sr-isotope measurements in the sandy layer (in MOZ3-CS06, at 5 to 6 cm, Table 4). Either the sedimentation is very condensed with an extremely low rate (less than 0.5 cm/Myr) in this sandy layer, or it indicates internal or sea floor erosions that are not visible in the core. Based on the location of these two cores, MOZ3-CS05 and MOZ3-CS06, sampling of the deposits from a drift aggradation phase (Miocene), it is reasonable to assume that an important part of the drift (thick aggradation) consists mainly of homogeneous muddy sedimentary facies, like those

collected in these two cores. This muddy sedimentation is consistent with sedimentation patterns observed in a separated mounded drift (e.g. Thiéblemont *et al.*, 2019; Miramontes *et al.*, 2021).

The three cores collected on the western flank of the ridge (MOZ3-CS03, MOZ3-CS02 and MOZ3-CS07) also show stratigraphy and sedimentation rates consistent with the interpretations of the geophysical data with a strong thinning of the deposits eastward (Fig. 14). The cores MOZ3-CS02 and MOZ3-CS03 are dominated by muddy deposits (clay and silty-clay grain size), interpreted as hemipelagic deposits (in grey in Figs 6, 7, 8 and 14). Some sandy layers indicate deposits of stronger energy. In core MOZ3-CS03, the erosive base, the normal grading, and the high content of quartz and feldspar minerals of sandy layers are consistent with turbidite deposits (Figs 7 and 10). No shallow-water bioclast is observed and the turbidity currents that generated these deposits were probably triggered on the submarine slope. In the sea floor morphology (Figs 2 and 4), the only channels visible are perpendicular to the slope, and are interpreted in relation to bottom current.

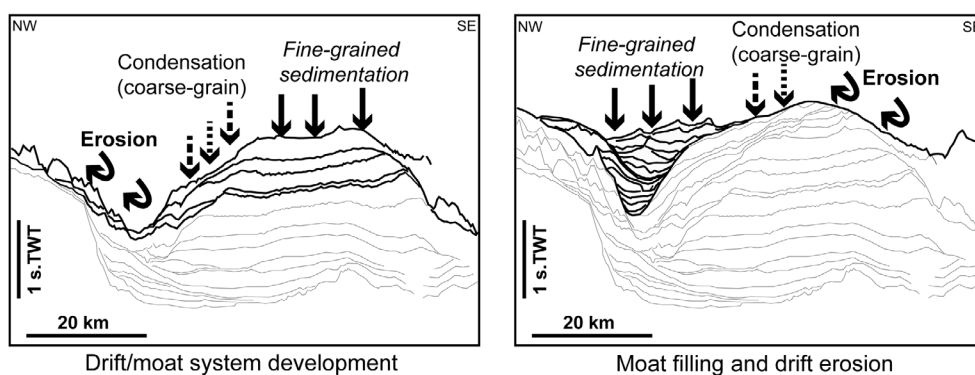


Fig. 15. Illustration of the two sedimentary behaviours observed on the Mozambique sedimentary ridge with the interpretation of the sediment distribution and erosion location.

However, the identification of channel–levée systems (Figs 3 and 14) is a possible indication of turbidity currents; but, in core MOZ3-CS03, turbidite deposits are rare and less than ten deposits over the last million years. They may be related to infrequent gravity instabilities on the upper slope, but probably do not represent an efficient turbiditic activity for the development of turbiditic channel–levée systems. In the Plio-Quaternary period, when the moat is filling up due to a weakening of the contour current, the moat could have captured and channelled small turbidity currents but this remains a minor contribution to the recent moat fill sedimentation.

In core MOZ3-CS02, the laminated sandy layer between 770 cm and 950 cm in the core (1.8 m thick) has different sedimentological characteristics from a turbidite (Figs 8 and 10); no clear base, no normal grading but numerous grain-size repetitive variations, and a composition dominated by foraminifera. This layer could have deposited over a long period of time and correlates with a 4 m thick sedimentary interval on the MOZ3-CS03 core according to the XRF signals (Fig. 12). The low content of muddy fraction and the numerous horizontal and oblique beddings indicate that this deposition occurred in the context of a continuous bottom current strong enough to prevent the deposition of fine-grained sediments.

The entire core MOZ3-CS07 is composed of calcareous sandy facies (from 60 to 75% of carbonates and from 12 to 25% of clay; Fig. 9), whose grains are mainly foraminifera (Fig. 10). The composition of this sediment consists of pelagic-sourced particles, and the low content of fine-grained sediment indicates a strong influence of bottom current. This influence consists

in winnowing away of the fine-grained particles and concentration of the approximately 200 to 800 μm bioclastic fraction, resulting in the deposition of a coarse-grained sedimentary facies with very low sedimentation rate about 0.3 cm/ka on core MOZ3-CS07 (Fig. 14).

This condensed facies (calcarenite or foraminiferal sand) described in cores MOZ3-CS02 and especially MOZ3-CS07, is associated with strong bottom currents and must be considered as a sandy contourite facies. Sediment condensation increases from MOZ3-CS03 (west) to MOZ3-CS07 (east) until there is no deposition and erosion at the top of the ridge. It is difficult to estimate the current velocity needed for moving particles such as foraminifera, as the density and shape of the particles varied and transport models are generally based on detrital grains, mainly quartz (McCave & Hall, 2006). It is accepted that the medium-sized foraminifera (planktonic and rounded) could be assimilated to elements of coarse silt or very fine sand (McCave, 2008). In the MOZ3 cores, foraminifera found in bioclastic sandy facies are probably not transported over long distances. The current velocity induces the removal of fine-grained particles (muddy fraction). According to McCave & Hall (2006), a velocity between 2 cm/s and 5 cm/s could allow winnowing away of mud and deposition of planktonic foraminifera.

Coarse-grained facies distribution in the contourite system

The sandy grain-size content evolves from 8% in MOZ3-CS03, where only a few sandy layers are interpreted as turbidite deposits, to 18% at core MOZ3-CS02 and to 100% in MOZ3-CS07.

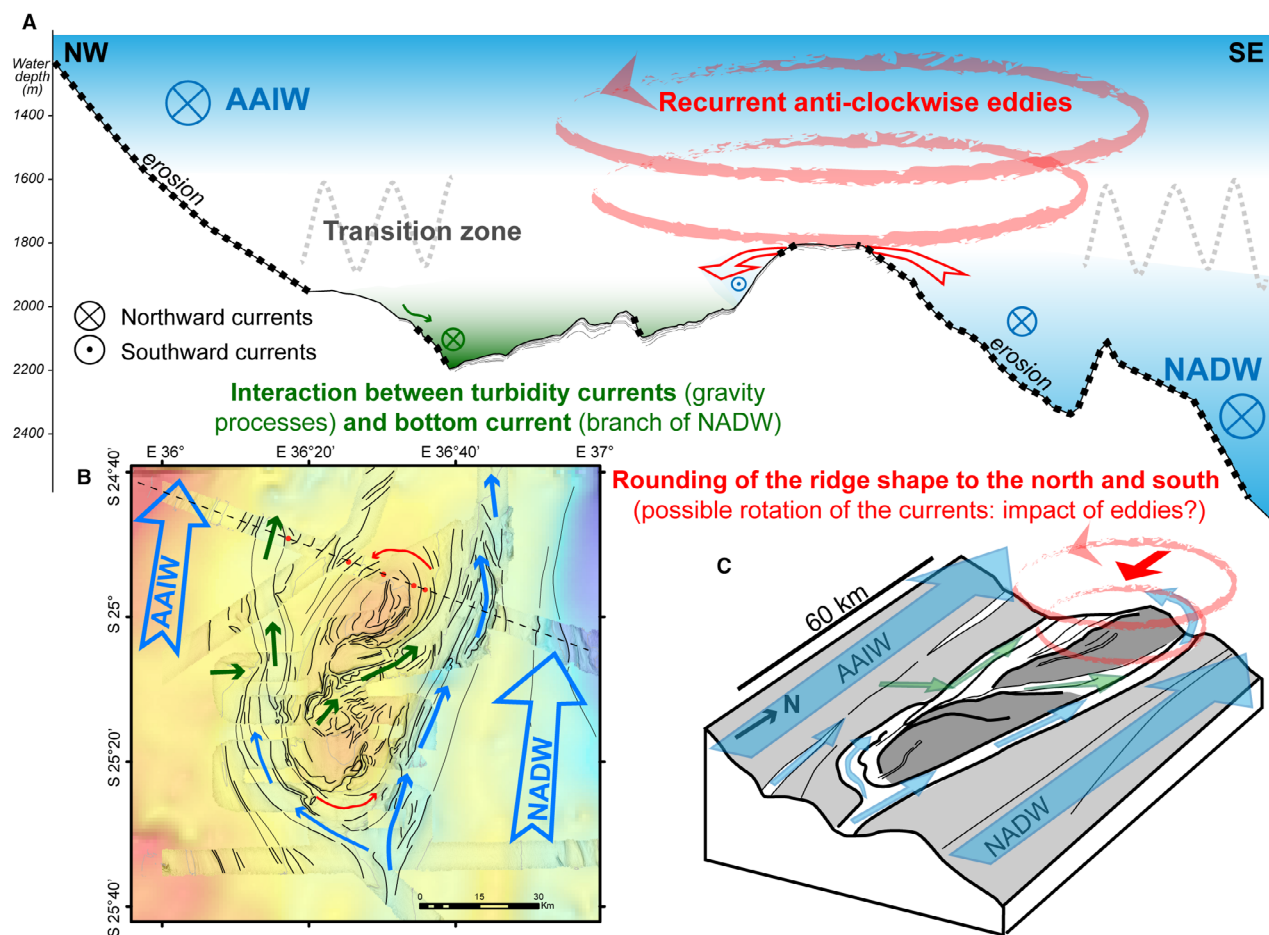


Fig. 16. (A) Interpretation of present processes on the profile across the ridge, (B) interpreted bathymetric map with probable current directions, and (C) schematic 3D illustration of the current trajectories and processes. Blue: main bottom currents; green: possible interactions of gravity processes (turbidity currents) with bottom currents; red: schematization of the possible impact of deep anti-clockwise eddies on the morphology of the bathymetric highs. AAIW – Antarctic Intermediate Water; NADW – North Atlantic Deep Water.

The coarse-grained contouritic facies is observed in two cores: MOZ3-CS02 (about 2 m thick) and MOZ3-CS07 (the whole core) and are interpreted as condensed facies. The depositional conditions of these coarse-grained facies are probably present in most contouritic systems in the intermediate position between erosional areas and depositional areas. They should be observable in the two configurations shown in Fig. 15: (i) between the moat and the drift during moat-drift system development; and (ii) during stages of drift/moat degradation when the moat is infilling and the drift is in erosion (Fig. 15). Areas of condensed sedimentation can also be identified in seismic profiles (or CHIRP profiles), where reflectors are close together, often sloping over the edges of drifts.

Present sedimentary and oceanographic processes

At present, the maximal water depth of the western channel is 2200 m and the top of the ridge is at 1800 m. In this water depth range, the study area is in the transition depths between the NADW (2200 to 3500 m) and AAIW (900 to 1500) both flowing northward. The maximum current velocities of the AAIW water mass are located on the upper slope (Figs 3 and 16). The erosion induced by this current on the upper slope is visible on the regional seismic profile in Fig. 3 (to a water depth of more than 1900 m; reported in Fig. 16). The erosion extends below the lower limit of the AAIW in the transition zone.

The bottom current linked to the NADW affects the lower part of the slope to the east of the study area. However, erosion is visible on the CHIRP profiles on the entire eastern flank of the ridge up to its summit at 1800 m depth (Figs 3, 4 and 15), higher than the NADW upper limit.

The transition between the two water masses is gradual and corresponds to slower velocities. Although there is no clear morphological criterion for interpreting the main direction of the currents in the east and west channels of the ridge, a dominant northerly direction is consistent with the general context and most observations.

The northward longitudinal slope in the western channel and the turbidite deposits observed in cores MOZ3-CS03 and MOZ3-CS02 are indicators of northward currents (gravity currents or mixed influence of gravity and bottom currents). In the same way, the direction of the erosion patterns between the bathymetric highs also indicate a north-eastern direction of the gravity currents probably under the influence of the top of the NADW in the eastern channel (Fig. 15). In the western channel, the influence of the NADW is possible but attenuated because the channel is above 2200 m depth (in the transition zone). The bottom current velocities are low enough to allow the deposition of fine hemipelagic sediments (as in MOZ3-CS03). However, these currents are not zero because erosional features and complex depositional shapes mark the axis of the western channel (lens-forms, significant changes in layer thickness), visible in particular on the chirp profiles (Fig. 4).

Regarding the general shape of the ridge (including the two bathymetric highs), the rounded morphology of the northern and southern edges does not correspond to a typical morphology in the context of a unidirectional northward flow (which should be more elongated and not rounded and eroded). This rounded and eroded shape can only be interpreted by assuming a deviation of the currents that will contour the submarine relief (Fig. 15). The rotation of the upper part of the NADW current that contours the north of the ridge and entered into the western channel southward was suggested by Miramontes *et al.* (2021) on the numerical bottom circulation model. This current would gradually diminish and imply a depositional zone in the western part of the ridge as observed on the profile and in the MOZ3-CS03 and MOZ3-CS02 cores. It may also be stronger and constant in velocity in the upper part of the ridge, explaining the sediment condensation in core MOZ3-CS07 and the erosion near

the top of the ridge. This process explains the rounded shape of the north side, but not the rounded shape of the south side, unless this current goes all the way around the ridge.

At the interface between two water masses, the current velocity is lower, and other oceanographic processes may interact with the sea floor, as the effect of internal tides, eddies, facilitating local erosion, resuspension and redistribution of sediment (Thiéblemont *et al.*, 2019). In the Mozambique Channel, large eddies have been shown to have an impact on the deep circulation (de Ruijter *et al.*, 2002; Halo *et al.*, 2014) and this impact is considered greater at transition zones between water masses (Thiéblemont *et al.*, 2019). The eddies which are known to be anti-clockwise and moving southward along the submarine slope are consistent in size and in location with the sedimentary patterns observed on the bottom. The base of eddies could be captured by the bathymetric highs (Fig. 15), but this remains rather hypothetical with the available data from this study.

Low oceanographic variability during the Quaternary in the study area

Sediment reworking processes by bottom-currents are often discontinuous or cyclic, depending on two main factors: variation in current velocity and variation in sediment influx (either detrital flux or fall-out of pelagic particles related to productivity). Variations in bottom currents may occur at very high frequency, for example, related to eddies (Yin *et al.*, 2019; Miramontes *et al.*, 2019c), but the first order cyclic control is relative sea-level change and climatic variations. The standard bi-gradational sequence defined by Gonthier *et al.* (1984) is often associated with variations in current intensity or sediment supply in relation to climatic cycles, particularly precession-driven changes (de Castro *et al.*, 2020b), but also at higher frequencies (for example, multicentennial scale; Martorelli *et al.*, 2021).

The stratigraphic and sedimentological study of the sediment cores of this study clearly shows that sedimentation at the three core sites (i.e. MOZ3-CS03 and MOZ3-CS07) is continuous with relatively stable sedimentation rates at each site. No bi-gradational sequences can be distinguished within sandy facies. Sedimentation thus appears relatively continuous over the last million years for MOZ3-CS03 and MOZ3-CS02 and surprisingly over about four to five million years for MOZ3-CS07 (Fig. 12).

The climatic and eustatic variations of the Quaternary (especially 100 kyr cycles) are well identified with the variations of O-isotopes of planktonic foraminifera in the MOZ3-CS03 core (Fig. 11) but are not directly identifiable in the sedimentary sequences and facies (visual description). The variations are also identified in the physical and chemical composition of the sediment, with significant variations in the lightness L^* , magnetic susceptibility, and Ca/Fe and Zr/Rb ratios. These variations in chemical composition allowed the stratigraphic calibration of the three cores (Fig. 12), which underlines the good continuity of the sedimentary signal. The homogeneity of the sedimentary facies and grain sizes indicate that the current intensity or water-mass depth are relatively stable during long periods covering several Quaternary climate cycles.

CONCLUSION

This work focused on a contourite sedimentary system located on the Limpopo Corridor in the southern part of the Mozambique margin, at water depth between 1800 m and 2200 m. The analysis of bathymetric data, sub-bottom profiler lines, a regional multichannel seismic profile and a transect of five sediment cores, provide a comprehensive study of this sedimentary system integrating different scales from the overall seismic structure down to the sedimentary facies and the recent processes.

At the seismic scale, three stages of contouritic sedimentation are distinguished on the margin since the Upper Cretaceous: (i) drift and moat development at the base of the slope escarpment from the Upper Cretaceous to the Eocene; (ii) an intermediate stage with successive phases of moat and upper-slope incisions alternating with aggradation during Oligocene and Miocene; and, finally, (iii) moat filling and erosion of the top of the ridge since the Pliocene.

The last stage is still ongoing with erosion of the eastern flank of the ridge and deposition in the moat. The sediment cores collected in the eastern flank of the ridge show that Miocene drift aggradation corresponds to calcareous muddy deposits. In the moat infill, muddy facies also dominate the sedimentation with sedimentation rates of about 1.4 to 1.7 cm/ka. Contouritic sandy facies are described in two cores with thick calcarenite layers showing bioturbations and laminations. It corresponds to condensed sedimentation with a low sedimentation rate about 0.2 to 0.3 cm/ka. The coarse-grained

contourite facies is mainly composed of bioclasts, particularly of planktonic foraminifera. The coarse-grained particles are concentrated by bottom currents that have winnowed away the fine-grained component of hemipelagic sedimentation. This type of facies could be present more generally in intermediate positions between erosional and depositional areas in contourite systems (and for example between moat and drift).

The piston cores cover stratigraphic records from one to several million years, showing that the current velocities are relatively stable over the last Quaternary climatic cycles. Currently, the sedimentary ridge is located in the transition zone between the North Atlantic Deep Water (NADW) and the Antarctic Intermediate Water (AAIW) masses. At this depth, currents are assumed to be weaker, the morphological and sedimentological analysis show that bottom currents have complex trajectories. Erosional patterns that contour the bathymetric highs indicate a significant influence of the upper part of the NADW, occasional turbidity currents in the moat, and possible impact of deep eddies on the sea floor morphology.

Although Plio-Quaternary depositional geometries indicate moat filling and drift erosion, sedimentary facies and processes are mostly driven by bottom currents. This work characterizes the contouritic sedimentation in the context of degradation of the drift/moat contourite system, with a multi-scale approach, allowing better understanding of the deep-marine sedimentary processes.

ACKNOWLEDGEMENTS

The PAMELA project (PASSive Margin Exploration Laboratories) is a scientific project led by Ifremer and TotalEnergies in collaboration with Université de Bretagne Occidentale, Université de Rennes 1, Université P&M Curie, CNRS and IFPEN. The authors thank the Captain and the crew of the PAMELA-MOZ03 survey onboard the *R/V Pourquoi Pas?* as well as INP and WesternGeco for their authorization to use multichannel seismic data image. We also thank the anonymous reviewers who helped to improve this article.

CONFLICT OF INTEREST

We declare that we have no commercial or associative aim that might represent a conflict of interest in connection with the work submitted.

DATA AVAILABILITY STATEMENT

The data that support the findings of this study are available from the corresponding author upon reasonable request.

REFERENCES

- Bankole, S., Buckman, J. and Stow, D. (2020) Unusual components within a fine-grained contourite deposit: significance for interpretation of provenance and the contourite budget. *Minerals*, **10**, 488.
- Brackenridge, R.E., Stow, D.A.V., Hernandez-Molina, F.J., Jones, C., Mena, A., Alejo, I., Ducassou, E., Llave, E., Ercilla, G., Nombela, M.A., Perez-Arlucea, M. and Frances, G. (2018) Textural characteristics and facies of sand-rich contourite depositional systems. *Sedimentology*, **65**, 2223–2252.
- Breitzke, M., Wiles, E., Krockner, R., Watkeys, M.K. and Jokat, W. (2017) Seafloor morphology in the Mozambique Channel: evidence for long-term persistent bottom-current flow and deep-reaching eddy activity. *Mar. Geophys. Res.*, **38**, 241–269.
- Charles, C., Pelleter, E., Révillon, S., Nonnotte, P., Jorry, S.J. and Kluska, J.M. (2020) Intermediate and deep ocean current circulation in the Mozambique Channel: new insights from ferromanganese crust Nd isotopes. *Mar. Geol.*, **430**, 106356.
- Coffin, M.F. and Rabinowitz, P.D. (1987) Reconstruction of Madagascar and Africa: evidence from the Davie fracture zone and western Somali basin. *J. Geophys. Res. Solid Earth*, **92**(B9), 9385–9406.
- Counts, J.W., Jorry, S.J., Leroux, E., Miramontes, E. and Jouet, G. (2018) Sedimentation adjacent to atolls and volcano-cored carbonate platforms in the Mozambique Channel (SW Indian Ocean). *Mar. Geol.*, **404**, 41–59.
- Davison, I. and Steel, I. (2018) Geology and hydrocarbon potential of the East African continental margin: a review. *Petrol. Geosci.*, **24**, 57–91.
- de Castro, S., Hernandez-Molina, F.J., de Weger, W., Jimenez-Espejo, F.J., Rodríguez-Tovar, F.J., Mena, A., Llave, E. and Sierro, F.J. (2020b) Contourite characterization and its discrimination from other deep-water deposits in the Gulf of Cadiz contourite depositional system. *Sedimentology*, **68**(3), 987–1027.
- de Castro, S., Hernandez-Molina, F.J., Rodríguez-Tovar, F.J., Llave, E., Ng, Z.L., Nishida, N. and Mena, A. (2020a) Contourites and bottom current reworked sands. *Mar. Geol.*, **428**, 106267.
- de Castro, S., Miramontes, E., Dorador, J., Jouet, G., Cattaneo, A., Rodríguez-Tovar, F.J. and Hernández-Molina, F.J. (2021) Siliciclastic and bioclastic contouritic sands: textural and geochemical characterisation. *Mar. Petrol. Geol.*, **128**, 105002.
- de Ruijter, W.P., Ridderinkhof, H., Lutjeharms, J.R., Schouten, M.W. and Veth, C. (2002) Observations of the flow in the Mozambique Channel. *Geophys. Res. Lett.*, **29**, 140–141.
- Donguy, J.R. and Piton, B. (1991) The Mozambique channel revisited. *Oceanol. Acta*, **14**, 549–558.
- Elderfield, H. (1986) Strontium isotope stratigraphy. *Palaeogeogr. Palaeoclimatol. Palaeoecol.*, **57**, 71–90.
- Evain, M., Schnürle, P., Leprêtre, A., Verrier, F., Watremez, L., Thompson, J.O., de Clarens, P., Aslanian, D. and Moulin, M. (2021) Crustal structure of the East-African Limpopo Margin, a strike-slip rifted corridor along the continental Mozambique Coastal Plain and North-Natal Valley. *Solid Earth Discussions*, **12**(8), 1865–1897.
- Faugères, J.C. and Stow, D.A.V. (2008) Contourite drifts: nature, evolution and controls. *Dev. Sedimentol.*, **60**, 257–288.
- Fierens, R., Droz, L., Toucanne, S., Raison, F., Jouet, G., Babonneau, N., Miramontes, E., Landurain, S. and Jorry, S.J. (2019) Late quaternary geomorphology and sedimentary processes in the Zambezi turbidite system (Mozambique Channel). *Geomorphology*, **334**, 1–28.
- Flemming, B.W. and Kudrass, H.-F. (2017) Large dunes on the outer shelf off the Zambezi Delta, Mozambique: evidence for the existence of a Mozambique Current. *Geo-Mar. Lett.*, **38**, 95–106.
- Gao, Y., Stow, D., Tang, Y., Xie, X. and Piper, D.J. (2020) Seismic stratigraphy and deep-water sedimentary evolution of the southern Mozambique margin: Central Terrace and Mozambique Fracture Zone. *Mar. Geol.*, **427**, 106187.
- Gonthier, E.G., Faugères, J.C. and Stow, D.A.V. (1984) Contourite facies of the Faro drift, Gulf of Cadiz. *Geol. Soc. Lond. Spec. Publ.*, **15**, 275–292.
- Halo, I., Backeberg, B., Penven, P., Ansonge, I., Reason, C. and Ullgren, J.E. (2014) Eddy properties in the Mozambique Channel: a comparison between observations and two numerical ocean circulation models. *Deep-Sea Res. II Top. Stud. Oceanogr.*, **100**, 38–53.
- Heaton, T.J., Köhler, P., Butzin, M., Bard, E., Reimer, R.W., Austin, W.E.N., Bronk Ramsey, C., Hughen, K.A., Kromer, B., Reimer, P.J., Adkins, J., Burke, A., Cook, M.S., Olsen, J. and Skinner, L.C. (2020) Marine20—the marine radiocarbon age calibration curve (0–55,000 cal BP). *Radiocarbon*, **62**, 779–820.
- Hernández-Molina, F.J., Llave, E. and Stow, D.A.V. (2008b) Continental slope contourites. In: *Contourites* (Eds Rebesco, M. and Camerlenghi, A.), pp. 379–408. Developments in Sedimentology, **60**. Elsevier, Amsterdam.
- Hernández-Molina, F.J., Maldonado, A. and Stow, D.A.V. (2008a) Abyssal plain contourites. In: *Contourites* (Eds Rebesco, M. and Camerlenghi, A.), pp. 345–378. Developments in Sedimentology, **60**. Elsevier, Amsterdam.
- Hernández-Molina, F.J., Sierro, F.J., Llave, E., Roque, C., Stow, D.A.V., Williams, T., Lofi, J., Van des Schee, M., Arnàiz, A., Ledesma, S., Rosales, C., Rodríguez-Tovar, F.J., Pardo-Iguzquiza, E. and Brackenridge, R.E. (2016) Evolution of the gulf of Cadiz margin and southwest Portugal contourite depositional system: tectonic, sedimentary and paleoceanographic implications from IODP expedition 339. *Mar. Geol.*, **377**, 7–39.
- Hüneke, H., Hernandez-Molina, F.J., Rodríguez-Tovar, F.J., Llave, E., Chiarella, D., Mena, A. and Stow, D.A.V. (2020) Diagnostic criteria based on microfacies for calcareous contourites, turbidites and pelagites in the Eocene-Miocene slope succession, southern Cyprus. *Sedimentology*, **68**(2), 557–592.
- Kolla, V., Eitrem, S., Sullivan, L., KostECKI, J.A. and Burckle, L.H. (1980) Current-controlled, abyssal microtopography and sedimentation in Mozambique Basin, Southwest Indian Ocean. *Mar. Geol.*, **34**, 171–206.
- Leinweber, V.T. and Jokat, W. (2012) The Jurassic history of the Africa–Antarctica corridor—new constraints from

- magnetic data on the conjugate continental margins. *Tectonophysics*, **530**, 87–101.
- Leprière, A., Schnürle, P., Evain, M., Verrier, F., Moorcroft, D., De Clarens, P., Corela, C., Afilhado, A., Loureiro, A., Leroy, S., d'Acremont, E., Thompson, J., Aslanian, D. and Moulin, M.** (2021) Deep structure of the North Natal Valley (Mozambique) using combined wide-angle and reflection seismic data. *J. Geophys. Res. Solid Earth*, **126**, e2020JB021171.
- Li, H., Tang, Y., Moulin, M., Aslanian, D., Evain, M., Schnurle, P., Leprière, A. and Li, J.** (2021) Seismic evidence for crustal architecture and stratigraphy of the Limpopo Corridor: new insights into the evolution of the sheared margin offshore southern Mozambique. *Mar. Geol.*, **435**, 106468.
- Lisiecki, L.E. and Raymo, M.E.** (2005) A Pliocene-Pleistocene stack of 57 globally distributed benthic $\delta^{18}O$ records. *Paleoceanography*, **20**, PA1003.
- Lutjeharms, J.R.E.** (2006) *The Agulhas Current*, Vol. 1. Springer-Verlag, Berlin.
- Maboya, M.L., Meadows, E.M., Reimer, P.J. and Backeberg, B.C.** (2017) Late Holocene marine radiocarbon reservoir correction for the southern and eastern coasts of South Africa. *Radiocarbon*, **60**, 571–582.
- Mahanjane, E.S.** (2014) The Davie Fracture Zone and adjacent basins in the offshore Mozambique Margin—a new insights for the hydrocarbon potential. *Mar. Petrol. Geol.*, **57**, 561–571.
- Martorelli, E., Bosman, A., Casalbore, D., Chiocci, F., Conte, A.M., Di Bella, L., Ercilla, G., Di Bella, L., Falcini, F., Falco, P., Frezza, V., Gaglianone, G., Giacco, B. and Mancini, M.** (2021) Mid-to-late Holocene upper slope contourite deposits off Capo Vaticano (Mediterranean Sea): high-resolution record of contourite cyclicity, bottom current variability and sandy facies. *Mar. Geol.*, **431**, 106372.
- McArthur, J.M.** (1994) Recent trends in strontium isotope stratigraphy. *Terra Nova*, **6**, 331–358.
- McCave, I.N.** (2008) Size sorting during transport and deposition of fine sediments: sortable silt and flow speed. In: *Contourites* (Eds Rebesco, M. and Camerlenghi, A.), Dev. Sedimentol., **60**, 121–142. Elsevier, Amsterdam.
- McCave, I.N. and Hall, I.R.** (2006) Size sorting in marine muds: processes, pitfalls and prospects for palaeoflow-speed proxies. *G-cubed*, **7**, Q10N05.
- Miramontes, E., Cattaneo, A., Jouet, G., Théreau, E., Thomas, Y., Rovere, M., Cauquil, E. and Trincardi, F.** (2016) The Pianosa contourite depositional system (northern Tyrrhenian Sea): drift morphology and Plio-Quaternary stratigraphic evolution. *Mar. Geol.*, **378**, 20–42.
- Miramontes, E., Garreau, P., Cattaneo, A., Caillaud, M., Jouet, G., Pellen, R., Hernández-Molina, F.J. and Clare, M.A.** (2019c) Contourite distribution in the NW Mediterranean Sea: new insights from hydrodynamic modelling. *Geomorphology*, **333**, 43–60.
- Miramontes, E., Jorry, S.J., Jouet, G., Counts, J.W., Courageon, S., Le Roy, P., Guérin, C. and Hernández-Molina, F.J.** (2019a) Deep-water dunes on drowned isolated carbonate terraces (Mozambique Channel, southwest Indian Ocean). *Sedimentology*, **66**, 1222–1242.
- Miramontes, E., Jouet, G., Thereau, E., Bruno, M., Penven, P., Guerin, C., Le Roy, P., Droz, L., Jorry, S.J., Hernández-Molina, F.J., Thiéblemont, A., Silva Jacinto, R. and Cattaneo, A.** (2020) The impact of internal waves on upper continental slopes: insights from the Mozambican margin (southwest Indian Ocean). *Earth Surf. Process. Landforms*, **45**, 1469–1482.
- Miramontes, E., Penven, P., Fierens, R., Droz, L., Toucanne, S., Jorry, S.J., Jouet, G., Pastor, L., Silva Jacinto, R., Gaillot, A., Giraudeau, J. and Raison, F.** (2019b) The influence of bottom currents on the Zambezi Valley morphology (Mozambique Channel, SW Indian Ocean): in situ current observations and hydrodynamic modelling. *Mar. Geol.*, **410**, 42–55.
- Miramontes, E., Thiéblemont, A., Babonneau, N., Penven, P., Raison, F., Droz, L., Jorry, S.J., Fierens, R., Counts, J.W., Wilckens, H., Cattaneo, A. and Jouet, G.** (2021) Contourite and mixed turbidite-contourite systems in the Mozambique Channel (SW Indian Ocean): link between geometry, sediment characteristics and modelled bottom currents. *Mar. Geol.*, **437**, 106502.
- Moulin, M. and Aslanian, D.** (2016) PAMELA-MOZ03 cruise, RV Pourquoi pas? <https://doi.org/10.17600/16001600>
- Moulin, M., Aslanian, D., Evain, M., Leprière, A., Schnurle, P., Verrier, F. and PAMELA-MOZ35 Team** (2020) Gondwana breakup: messages from the North Natal Valley. *Terra Nova*, **32**, 205–214.
- Mueller, C.O. and Jokat, W.** (2019) The initial Gondwana break-up: a synthesis based on new potential field data of the Africa-Antarctica Corridor. *Tectonophysics*, **750**, 301–328.
- Nairn, A.E., Lerche, I. and Iliffe, J.E.** (1991) Geology, basin analysis, and hydrocarbon potential of Mozambique and the Mozambique Channel. *Earth-Sci. Rev.*, **30**, 81–123.
- Penven, P., Halo, I., Pous, S. and Marié, L.** (2014) Cyclogeostrophic balance in the Mozambique Channel. *J. Geophys. Res. Oceans*, **119**, 1054–1067.
- Ponte, J.P., Robin, C., Guillocheau, F., Popescu, S., Suc, J.P., Dall'Asta, M., Melinte-Dobrinescu, M.C., Bubik, M., Dupont, G. and Gaillot, J.** (2019) The Zambezi delta (Mozambique channel, East Africa): high resolution dating combining bio-orbital and seismic stratigraphy to determine climate (palaeoprecipitation) and tectonic controls on a passive margin. *Mar. Pet. Geol.*, **105**, 293–312.
- Raillard, S.** (1991). Les marges de l'Afrique de l'Est et les zones de fractures associées Chaîne Davie et ride du Mozambique, thèse de doctorat de l'Université de Grenoble.
- Rebesco, M., Hernández-Molina, F.J., van Rooij, D. and Wählin, A.** (2014) Contourites and associated sediments controlled by deep-water circulation processes: state-of-the-art and future considerations. *Mar. Geol.*, **352**, 111–154.
- Richter, T.O., Van der Gaast, S., Koster, B., Vaars, A., Gieles, R., de Stigter, H.C., de Haas, H. and van Weering, T.C.** (2006) The Avaatech XRF Core Scanner: technical description and applications to NE Atlantic sediments. *Geol. Soc. Lond. Spec. Publ.*, **267**, 39–50.
- Ridderinkhof, H., Van der Werf, P.M., Ullgren, J.E., Van Aken, H.M., Van Leeuwen, P.J. and de Ruijter, W.P.M.** (2010) Seasonal and interannual variability in the Mozambique Channel from moored current observations. *J. Geophys. Res. Oceans*, **115**, C06010.
- Rodrigues, S., Hernández-Molina, F.J., Fonnesu, M., Miramontes, E., Rebesco, M. and Campbell, D.C.** (2022) A new classification system for mixed (turbidite-contourite) depositional systems: examples, conceptual models and diagnostic criteria for modern and ancient records. *Earth-Sci. Rev.*, **230**, 104030.

- Sansom, P.** (2018) Hybrid turbidite–contourite systems of the Tanzanian margin. *Petrol. Geosci.*, **24**, 258–276.
- Schouten, M.W., De Ruijter, W.P. and Van Leeuwen, P.J.** (2002) Upstream control of Agulhas Ring shedding. *J. Geophys. Res. Oceans*, **107**(C8), 23–21.
- Schouten, M.W., de Ruijter, W.P., Van Leeuwen, P.J. and Ridderinkhof, H.** (2003) Eddies and variability in the Mozambique Channel. *Deep-Sea Res. II Top. Stud. Oceanogr.*, **50**, 1987–2003.
- Stow, D.A., Faugères, J.C., Howe, J.A., Pudsey, C.J. and Viana, A.R.** (2002) Bottom currents, contourites and deep-sea sediment drifts: current state-of-the-art. *Geol. Soc. Lond. Mem.*, **22**, 7–20.
- Stow, D.A.V. and Faugères, J.C.** (2008) Contourite facies and the facies model. *Dev. Sedimentol.*, **60**, 223–256.
- Stow, D.A.V., Hernández-Molina, F.J., Llave, E., Sayago, M., Díaz del Río, V. and Branson, A.** (2009) Bedform-velocity matrix: the estimation of bottom current velocity from bedform observations. *Geology*, **37**, 327–330.
- Stow, D.A.V. and Smillie, Z.** (2020) Distinguishing between deep-water sediment facies: turbidites, contourites and hemipelagites. *Geosciences*, **10**, 68.
- Stuiver, M., Reimer, P.J. and Braziunas, T.F.** (1998) High-precision radiocarbon age calibration for terrestrial and marine samples. *Radiocarbon*, **40**, 1127–1151.
- Thiéblemont, A., Hernández-Molina, F.J., Miramontes, E., Raison, F. and Penven, P.** (2019) Contourite depositional systems along the Mozambique channel: the interplay between bottom currents and sedimentary processes. *Deep-Sea Res. I Oceanogr. Res. Pap.*, **147**, 79–99.
- Thiéblemont, A., Hernandez-Molina, F.J., Ponte, J.P., Robin, C., Guillocheau, F., Cazzola, C. and Raison, F.** (2020) Seismic stratigraphic framework and depositional history for Cretaceous and Cenozoic contourite depositional systems of the Mozambique Channel, SW Indian Ocean. *Mar. Geol.*, **425**, 106192.
- Thompson, J.O., Moulin, M., Aslanian, D., De Clarens, P. and Guillocheau, F.** (2019) New starting point for the Indian Ocean: second phase of breakup for Gondwana. *Earth Sci. Rev.*, **191**, 26–56.
- Uenzelmann-Neben, G. and Huhn, K.** (2009) Sedimentary deposits on the southern South African continental margin: slumping versus non-deposition or erosion by oceanic currents? *Mar. Geol.*, **266**, 65–79.
- Ullgren, J.E., van Aken, H.M., Ridderinkhof, H. and de Ruijter, W.P.M.** (2012) The hydrography of the Mozambique Channel from six years of continuous temperature, salinity, and velocity observations. *Deep Sea Res. Oceanogr. Res. Pap.*, **69**, 36–50.
- van Aken, H.M., Ridderinkhof, H. and de Ruijter, W.P.M.** (2004) North Atlantic deep water in the south-western Indian Ocean. *Deep-Sea Res. I Oceanogr. Res. Pap.*, **51**, 755–776.
- Watremez, L., Leroy, S., d'Acremont, E., Roche, V., Evain, M., Leprière, A., Verrier, F., Aslanian, D., Dias, N., Afilhado, A., Schnürle, R., Castilla, R., Despinois, F. and Moulin, M.** (2021) The limpopo magma-rich transform margin, South Mozambique: 1. Insights from deep-structure seismic imaging. *Tectonics*, **40**(12), e2021TC006915.
- Wiles, E., Green, A., Watkeys, M., Jokat, W. and Krocker, R.** (2014) Anomalous seafloor mounds in the northern Natal Valley, southwest Indian Ocean: implications for the East African Rift System. *Tectonophysics*, **630**, 300–312.
- Wiles, E., Green, A.N., Watkeys, M.K. and Jokat, W.** (2017) Zambezi continental margin: compartmentalized sediment transfer routes to the abyssal Mozambique Channel. *Mar. Geophys. Res.*, **38**, 227–240.
- Yin, S., Hernández-Molina, F.J., Zhang, W., Li, J., Wang, L. and Ding, W.** (2019) The influence of oceanographic processes on contourite features: a multidisciplinary study of the northern South China Sea. *Mar. Geol.*, **415**, 105967.
- Yu, X., Stow, D., Smillie, Z., Esentia, I., Brackenridge, R., Xie, X., Bankole, S., Ducassou, E. and Llave, E.** (2020) Contourite porosity, grain size and reservoir characteristics. *Mar. Petrol. Geol.*, **117**, 104392.

Manuscript received 6 March 2022; revision accepted 12 September 2022